

Jets in strongly-coupled $\mathcal{N} = 4$ super Yang-Mills theory

Paul M. Chesler*, Kristan Jensen†, and Andreas Karch‡
Department of Physics, University of Washington, Seattle, WA 98195, USA
(Dated: October 28, 2018)

We study jets of massless particles in $\mathcal{N} = 4$ super Yang-Mills using the AdS/CFT correspondence both at zero and finite temperature. We set up an initial state corresponding to a highly energetic quark/anti-quark pair and follow its time evolution into two jets. At finite temperature the jets stop after traveling a finite distance, whereas at zero temperature they travel and spread forever. We map out the corresponding baryon number charge density and identify the generic late time behavior of the jets as well as features that depend crucially on the initial conditions.

I. INTRODUCTION

In a hadronic collider such as the LHC, most interesting processes involve final states with jets of hadrons or equivalently, sprays of particles heading in roughly the same direction within a certain opening angle. The data available to define and reconstruct the jets are energy depositions in the calorimeter and charged particle tracks. Ideally one can use this experimental data to identify an underlying hard scattering event that involved QCD partons in the weakly coupled high energy regimes or, alternatively, heavy standard model particles such as top quarks or newly produced non-standard model particles. Distinguishing the former from the latter is of course crucial to our ability to find and analyze new physics at the LHC.

Despite its obvious importance, several aspects of jet physics are still in need of better understanding. A large portion of the current understanding of jets comes from perturbative techniques. For a recent review see Ref [1]. First, a jet has to be defined via one of several algorithms, all of which have their own benefits and problems. The properties of the jet then have to be compared to a perturbative calculation of the hard scattering. The initial hard scattering however has to be first processed by a parton shower routine that evolves every hard parton into a jet of partons which eventually hadronize into baryons and mesons. The distribution of the latter can then be matched with the experimentally observed data. This compartmentalization of the theoretical part into three stages assumes that these processes, which are governed by physics at very different energy scales, happen independently. This is the statement of factorization. While resummed perturbation theory or soft collinear effective theory give a theoretical handle on the showering, Monte Carlo simulations based on models (and not QCD) are often employed for this step. The hadronization is always handled by phenomenological models. One question we will address in this work is how the process of showering occurs in a particular solvable toy model of strong

coupling dynamics. In particular, we study jets in large N_c , $SU(N_c)$ $\mathcal{N} = 4$ super-Yang-Mills (SYM) at strong 't Hooft coupling λ where the process has a dual description in terms of a string falling in a $5d$ geometry. This may help us understand what aspects of showering are genuinely QCD and may also lead to better models of showering.

A quite different experimental setting that prominently features jets are heavy ion colliders, such as the currently operating RHIC experiment as well as the heavy-ion runs that will take place part of the time at the LHC. The goal of these experiments is not so much to find physics beyond the standard model but rather to explore the phase structure of QCD at high temperatures. At the temperatures achieved in the RHIC collisions, quarks and gluons are thought to be liberated although not free. Their collective dynamics are well described by an almost perfect fluid [2, 3]. Jets, which are produced by hard collisions within the expanding fireball, serve as a probe of the interior of the plasma. In this context one wants to know the rate at which jets lose energy and broaden when traversing the medium. These are strongly coupled non-equilibrium phenomena and are therefore challenging for both the lattice and for diagrammatic approaches. Again, it is helpful to have a solvable toy model. We will study jets of massless quarks traversing a finite temperature plasma in the same solvable toy model, $\mathcal{N} = 4$ SYM at strong coupling.

Our approach, both at zero and finite temperature, is to prepare at a state at time $t = 0$ which is well described by a semi-classical wave-function. In the gravity dual, this corresponds to a classical string moving in the dual geometry. At $t = 0$ we specify the initial configuration of the string and let it time evolve according to the equations of motion that follow from the Nambu-Goto action. The time evolution of the string is dual to the evolution of baryon and energy densities in the corresponding field theory state. A similar approach has been used to study the properties of jets of massive matter in the same theory at zero temperature [4, 5] and finite temperature [5]. In this work, we compute the evolution of baryon density at both zero and finite temperature for the case of massless quarks. For concreteness, we consider states with two back to back jets. In particular, we consider string states where the string profile lies in one Minkowski spatial direction. However our analysis and results for the

* Email: pchesler@u.washington.edu

† Email: kristanj@u.washington.edu

‡ Email: karch@phys.washington.edu

baryon density are easily generalized to the case where the string profile extends in more than one Minkowski spatial direction.

For the classical description to be valid the string must carry large conserved charges. In particular, the energy of the string scales as $\sqrt{\lambda}$. At finite temperature, this setup is very well suited for the question of studying the energy and momentum loss rates of an energetic projectile traversing the medium. Our calculation generalizes the calculation of the heavy quark energy loss rate of [6, 7] to the case of massless quarks. The additional complication is that for massless quarks the plasma can transport the charge and so the initially localized charge distribution eventually diffuses; the string falls. While we don't have a conclusive answer on the loss rate and stopping distance yet, our simulations indicate that a recent analysis of this process based purely on the analysis of geodesics [8] is incomplete. One of the central results of our numerical investigations is that the endpoint motion indeed very quickly settles onto a lightlike geodesic for generic initial conditions. However the relation between the energy of the quark and the parameters specifying the geodesic can be more complicated than presented in [8].

At zero temperature our approach is new, even though the situation is quite similar in spirit to the case of finite temperature. At time $t = 0$ we prepare a quark/antiquark pair with enough kinetic energy to climb out of each others' potential well. We follow in detail the evolution of the baryon number density and can in principle do the same for energy densities. As each one of the energetic projectiles moves through the vacuum, both densities spread so that instead of two single well defined particles flying back-to-back at the speed of light, we see narrow distributions of baryon number density within two cones around the directions of the original quark/antiquark pair — a pair of jets. The dynamical mechanism underlying this jet formation from the field theory perspective seems to be the emission of a large number of soft gluons and quarks. This setup with an initial semi-classical state whose subsequent evolution is studied mirrors closely the usual factorization framework. An initial hard scattering event will have to produce the $t = 0$ string configuration. We do not specify the dynamics that gave rise to the initial configuration. In any case, this would have to be very different from QCD where the initial hard event is perturbative. The subsequent showering is what we study using the gravity dual. The conformal theory itself doesn't hadronize, but gravity duals for confining gauge theories are known. In these cases only the deep interior of the geometry is modified. This will not modify the initial falling stage of the string motion. Factorization of the showering stage from the hadronization stage is guaranteed by bulk locality in our setup.

This approach is rather different from the recent work in [9]. There the authors study the evolution of a vector wavepacket as it falls into an AdS geometry. The

dynamics of the falling wavepacket are dual to the evolution of an R -charge jet in the same theory that we study, $\mathcal{N} = 4$ SYM at strong coupling. In contrast, we study jets of fundamental matter with large energies that scale like $\sqrt{\lambda}$.

An alternative approach to studying jets is to consider observables which are completely self contained and do not refer to a particular initial state. The best theoretically motivated observables are the energy correlators introduced in [10, 11, 12]. In a state obtained from acting with a local current on the vacuum, the energy density one-point function exhibits an “antenna pattern” where the number of particles heading into a particular direction is correlated with the polarization of the current, giving rise to an intrinsically jet-like event. These antenna patterns have recently been studied in [13] for strongly coupled $\mathcal{N} = 4$ (in fact for any CFT) and it was found that in a theory with a supergravity dual they are perfectly spherical and show no sign of jet-like structure.¹ A different question is to ask about the likelihood that an initial off shell photon would produce a quark/antiquark pair with a particular preferred axis. The result of [13] shows that an off shell photon would produce quark/antiquark pairs with no preferred axis and on top of this no correlation between the direction of the quark and the antiquark. In contrast, we set up an initial state that has a preferred direction for both. We mostly focus on back-to-back jets, but as we show in Section IV, our methods apply for quarks and antiquarks heading in completely different directions. The results of [13] then simply implies that the initial states we consider are not created by a local $\mathcal{N} = 4$ current operator. Again, we emphasize that this is not a concern for the issue of studying showering as the dynamics that give rise to the creation of a $q\bar{q}$ state via the decay of an energetic off-shell photon are qualitatively different in a strongly-coupled conformal theory than QCD, which is asymptotically free.

The framework that allows us to do these calculations is the AdS/CFT correspondence [16, 17, 18]. In the limit $N_c \rightarrow \infty$ and $\lambda \gg 1$, $\mathcal{N} = 4$ SYM has a dual description in terms of type IIB supergravity on an AdS_5 or AdS_5 black hole geometry times an internal 5-sphere. In addition, states with an energy scaling as $\sqrt{\lambda}$ can be described by a classical Nambu-Goto string moving in this spacetime, as is implicit in the calculation of Wilson line expectation values of [19, 20] and was argued in detail in [21]. Similarly, we consider a state that consists of an open string which is created at a point in space at time $t = 0$. Such initial conditions locally conserve charge in the bulk and baryon number on the boundary. As shown in Fig. 1, as time evolves the string evolves from a point into an extended object and falls under the influence of gravity. The string's endpoints are charged under a $U(1)$ gauge field \mathcal{A}_M . The simplest realization of such a gauge

¹ This result had been anticipated in [4, 14, 15].

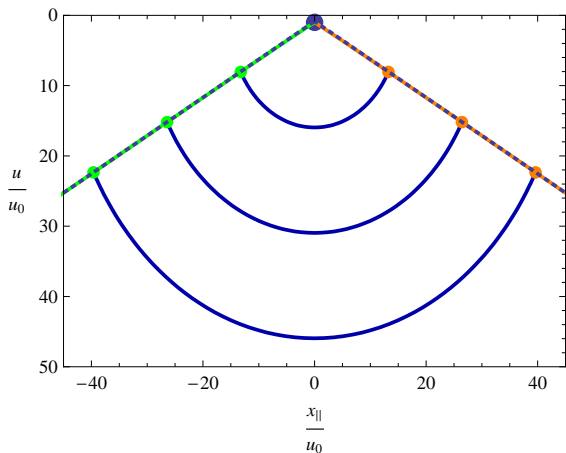


FIG. 1: A plot of a falling string at zero temperature. The string is created at radial coordinate $u = u_0$ and expands as it falls. The endpoint trajectories, shown in the figure as solid green and orange lines, asymptotically approach light-like geodesics which are shown in the figure as dotted blue lines.

field is the worldvolume gauge field of a D7 flavor brane, which is spacetime filling from the 5d point of view and wraps a 3-sphere in the internal S^5 . According to [22] the addition of such a flavor brane from the field theory point of view corresponds to the addition of an $\mathcal{N} = 2$ supersymmetric hypermultiplet in the fundamental representation of the $SU(N_c)$ gauge group.

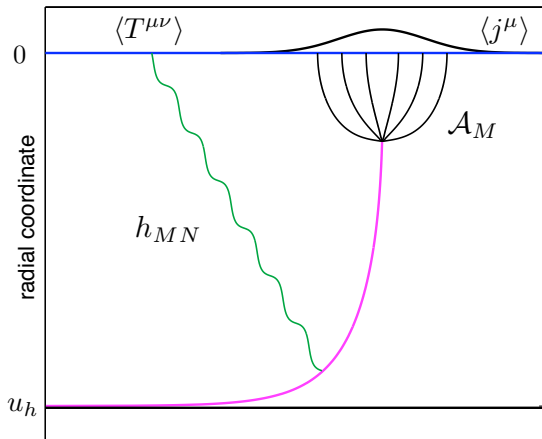


FIG. 2: A cartoon of the bulk to boundary problem at finite temperature. The endpoints of strings are charged under a $U(1)$ gauge field \mathcal{A}_M . The boundary of the geometry, located at radial coordinate $u = 0$, behaves like a perfect conductor and consequently, the presence of the string endpoints induces a mirror current density j^μ on the boundary. Via the AdS/CFT correspondence, the induced current density has the interpretation of the baryon current of a jet. Similarly, the presence of the string induces a perturbation h_{MN} in the metric of the bulk geometry. The behavior of the metric perturbation near the boundary encodes the information contained in the perturbation in the SYM stress tensor due to the presence of the jet.

In the large N_c limit the coupling e^2 between the gauge field \mathcal{A}_M and the string scales as $e^2 \sim 1/N_c$ and consequently the backreaction of the gauge field on the string's motion can be neglected. Similarly, in the large N_c limit the 5d gravitational constant $\kappa_5^2 \sim 1/N_c^2$ so the backreaction of gravity on the string can be neglected too. In short, in the large N_c limit the string falls freely under the influence of gravity and the behavior of the gauge field \mathcal{A}_M (and the perturbation to the metric h_{MN} caused by the string) can be computed perturbatively. The dual field theory lives on the boundary of the asymptotically AdS geometry. The boundary behaves like an ideal electromagnetic conductor, so the presence of the gauge field \mathcal{A}_M induces a current $j^\mu(x)$ which resides purely on the boundary. This is depicted schematically in Fig. 2. Via the AdS/CFT correspondence, this induced current has the physical interpretation of the baryon current density of a quark-antiquark pair. Similarly, the boundary behavior of the metric perturbation induces a perturbation in the boundary stress-energy tensor $T^{\mu\nu}$. The perturbation in $T^{\mu\nu}$ contains both the stress-energy of the quarks and the stress-energy of any emitted radiation.

At zero temperature we show that the string endpoint trajectories generically approach light-like geodesics at late times. While the baryon density at any point on the boundary may be sensitive to the behaviour of the source before it relaxes to geodesic motion, we are able to find boundary observables that are insensitive to early time dynamics. In particular, we find that the center of charge and the angular distribution of baryon number are uniquely determined in terms of a single parameter V_s , which is the asymptotic spatial velocity of the string endpoint. The angular distribution of baryon number falls off as $\frac{1}{(1-V_s \cos \theta)^2}$ with the angle θ measured relative to the main axis of the jet.

At finite temperature we consider string configurations where the string endpoints travel very far in the spatial directions. To generate such configurations, the strings must start very close to the boundary of the AdS-BH geometry and must have a very high energy and momentum. For such string configurations, we find that the endpoint motion is approximately geodesic even at early times. The corresponding baryon density can be made highly localized for a period of time and hence can be considered to be the baryon density of a quasi particle. We track the evolution of the baryon density from the initial event where a quark-antiquark pair was created to thermalization of the resulting jets and the onset of hydrodynamics.

An outline of our paper is as follows. In Section I A we write down the conventions we use. In Section II we discuss the dynamics of falling strings at both zero temperature and finite temperature. In both cases approximate analytic solutions to the string equations of motion are constructed and in both cases we perform numerical studies of the string solutions. In Section III we study the 5d electromagnetic problem and compute the baryon density induced in the boundary field theory.

In Section IV we discuss the implications of our results and in Section V we conclude.

A. Conventions

Five dimensional AdS coordinates will be denoted by X_M while four dimensional Minkowski coordinates will be denoted by x_μ . Upper case Latin indices M, N, P, \dots run over $5d$ AdS coordinates, while Greek indices run over the $4d$ Minkowski space coordinates. Worldsheet coordinates will be denoted as σ^a with $a = 0, 1$. The time like world sheet coordinate is $\tau \equiv \sigma^0$ while the spatial coordinate is $\sigma \equiv \sigma^1$. The endpoints of the string are located at $\sigma = \sigma^*$. We choose coordinates such that the metric of the AdS-Schwarzschild (AdS-BH) geometry is

$$ds^2 = \frac{L^2}{u^2} \left[-f(u) dt^2 + d\mathbf{x}^2 + \frac{du^2}{f(u)} \right], \quad (1.1)$$

where $f(u) \equiv 1 - (u/u_h)^4$ and L is the AdS curvature radius. The coordinate u is an inverse radial coordinate; the boundary of the AdS-BH spacetime is at $u = 0$ and the event horizon is located at $u = u_h$, with $T \equiv (\pi u_h)^{-1}$ the temperature of the SYM plasma.

II. FALLING STRINGS

The dynamics of a classical string are governed by the Nambu-Goto action

$$S_{\text{NG}} = -T_0 \int d\tau d\sigma \sqrt{-\gamma} \quad (2.1)$$

where $T_0 = \sqrt{\lambda}/2\pi L^2$ is the string tension, σ and τ are worldsheet coordinates and $\gamma = \det \gamma_{ab}$ with γ_{ab} the induced worldsheet metric. The string profile is determined by a set of embedding functions $X^M(\tau, \sigma)$. In terms of these functions we have

$$\gamma_{ab} = \partial_a X \cdot \partial_b X, \quad (2.2)$$

and

$$-\gamma = (\dot{X} \cdot X')^2 - \dot{X}^2 X'^2 \quad (2.3)$$

where $\dot{X}^M \equiv \partial_\tau X^M$ and $X'^M \equiv \partial_\sigma X^M$.

The equations of motion for the embedding functions and the open string boundary conditions follow from setting the variation of the Nambu-Goto action to vanish. We write the equations of motion below in Sections II A 1 and II A 2. The open string boundary conditions require the string endpoints to move at the local speed of light and that their motion is transverse to the string.

We consider initial conditions such that at worldsheet time $\tau = 0$, the string is mapped into a single point in space. We furthermore consider string profiles which lie

in the Minkowski spatial direction $x \equiv x_{||}$. The point-like initial conditions are

$$t(0, \sigma) = 0, \quad x(0, \sigma) = 0, \quad u(0, \sigma) = u_0. \quad (2.4)$$

The remaining necessary initial data is that of \dot{t} , \dot{x} and \dot{u} at $\tau = 0$. However one of these three functions may be eliminated via gauge fixing. For example one may choose to work in the gauge $\tau = t$. We leave the detailed discussion of our particular choice of the remaining initial data for Section II B. We simply note here that we can choose initial conditions such that (i) at zero temperature the string endpoints move infinitely far apart as $t \rightarrow \infty$ and, (ii) at finite temperature the initial conditions can be chosen such that the endpoints travel an arbitrarily large (but finite) distance in the Minkowski spatial directions. As discussed in Section III, at zero temperature strings whose endpoints separate to spatial infinity correspond to jets in the dual field theory. At finite temperature, strings whose endpoints can be made to travel arbitrarily far in the Minkowski spatial directions correspond to quasi-particle states in the dual field theory.

A. Approximate Solutions

At both zero temperature and finite temperature it is possible to obtain approximate solutions to the string equations of motion. Our zero temperature solution is valid in the $t \rightarrow \infty$ limit. Such a limit is meaningful to consider at zero temperature as the string solutions will expand indefinitely and will correspond to jets in the dual field theory which separate forever. At finite temperature, the $t \rightarrow \infty$ limit of string solutions is not a useful limit to consider. This is because at finite temperature strings will fall asymptotically close to the black hole as time progresses. This corresponds to the thermalization of jets in the dual field theory. At finite temperature we perform an expansion which in essence corresponds to studying an arbitrarily high energy string.

Both zero temperature and finite temperature approximations rely on the fact that there exist exact solutions to the string equations of motion where the string is everywhere moving at the speed of light. Such solutions have infinite energy and hence are unphysical by themselves, but nevertheless serve as good solutions to base an asymptotic expansion around. In our numeric studies shown below in Section II B, we demonstrate excellent agreement between our asymptotic solutions and the exact numerical solutions for a wide class of initial conditions.

1. Zero Temperature

To obtain the $T = 0$ late time asymptotic solutions, we choose worldsheet coordinates such that $\tau = t$ and

$\sigma = \varphi$ where φ is an angular coordinate defined by

$$x = \ell(t, \varphi) \cos \varphi \quad (2.5)$$

$$u = \ell(t, \varphi) \sin \varphi. \quad (2.6)$$

The domain in the (t, φ) plane in which $\ell(t, \varphi)$ is defined is bounded by two curves $\varphi_s(t)$, $s = 1, 2$. These curves correspond to the motion of the string endpoints and are determined by imposing the open string boundary conditions. The open string boundary conditions require the endpoints to move at the speed of light and for the endpoint velocity to be transverse to the string. This implies that along the curves $\varphi_s(t)$

$$G_{MN} \frac{dX^M}{dt} \frac{dX^N}{dt} = 0, \quad (2.7)$$

$$G_{MN} \frac{dX^M}{dt} \frac{\partial X^N}{\partial \varphi} = 0 \quad (2.8)$$

The equation of motion for $\ell(t, \varphi)$ is

$$\begin{aligned} \ell^2(\ell^2 + \ell'^2)\ddot{\ell} - \ell^2(1 - \dot{\ell}^2)\ell'' + 2\ell^2\ell' \cot \varphi + 2\ell'^3 \cot \varphi \\ - 2\ell^2\dot{\ell}\ell'(\dot{\ell} \cot \varphi + \dot{\ell}') - \ell^3(1 - \dot{\ell}^2) = 0. \end{aligned} \quad (2.9)$$

Generic open string solutions to the above equation will fall forever into the bulk of the AdS geometry and will approach the speed of light. In particular, ℓ will generically scale like t at late times. Because we are interested in string solutions which correspond to jets in the dual field theory, we seek solutions whose endpoint separation in the spatial directions also grows like t in the large t limit. Such string solutions will expand at a rate approaching the speed of light, and correspondingly, as time progresses neighboring points on string will become causally disconnected. Just as in inflation, any short wavelength structure in the string will expand and become long wavelength at late times and correspondingly, $\ell'/\ell \rightarrow 0$ as $t \rightarrow \infty$.

Our starting point for the $T = 0$ late time asymptotics is to expand $\ell(t, \varphi)$ in an asymptotic expansion about $t = \infty$. We write

$$\ell(\varphi, t) = \chi(\varphi)t + \sum_{n=0}^{\infty} \ell_n(\varphi)t^{-n}. \quad (2.10)$$

Using the assumption that $\ell'/\ell \rightarrow 0$ as $t \rightarrow \infty$, one can conclude that $\chi(\varphi) = \text{constant}$. However for completeness we choose to demonstrate that this is the unique solution to the equations of motion which satisfies the open string boundary conditions.

Consistency of the above asymptotic expansion (2.10) with the boundary conditions in Eqs. (2.7)–(2.8) implies that the functions $\varphi_s(t)$ must have the asymptotic expansions

$$\varphi_s(t) = \sum_{n=0}^{\infty} \varphi_n^s t^{-n}. \quad (2.11)$$

Note that this expansion does not contain any positive powers of t . Any positive powers of t in the expansion of $\varphi_s(t)$ would imply superluminal motion for the endpoints.

Substituting the expansion (2.10) into the equation of motion (2.9) and setting the leading coefficient in the large t expansion to vanish, we find the following equation for $\chi(\varphi)$

$$\begin{aligned} -\chi(1 - \chi^2)\chi'' + 2(\chi')^3 \cot \varphi - 2\chi^3(\chi')^2 \\ - (1 - \chi^2)(1 - 2\chi^2\chi' \cot \varphi) = 0. \end{aligned} \quad (2.12)$$

Similarly, substituting the expansions into the boundary conditions (2.7) and (2.8) and setting the leading coefficient in the large t expansion to vanish, we find the following equations

$$\chi(\varphi_0^s) = 1, \quad (2.13)$$

$$\chi'(\varphi_0^s) = 0. \quad (2.14)$$

As advertised, the solution to Eq. (2.12) which satisfies the above boundary conditions is simply

$$\chi(\varphi) = 1. \quad (2.15)$$

We note that the leading order solution $\ell = t$ represents a null string with $\gamma = 0$. This solution simply represents an arc which uniformly expands at the speed of light.

At next to leading order in the $1/t$ expansion, we find the following equation of motion

$$\ell_0\ell_1 + \ell_2 + 2\ell'_0\ell_1 \cot \varphi + (\ell'_0)^3 \cot \varphi + \ell'_0\ell'_1 - \ell_1\ell''_0 = 0. \quad (2.16)$$

The solution to the above equation simply relates ℓ_2 to ℓ_0 and ℓ_1 via an algebraic equation. This feature also occurs at higher orders in the $1/t$ expansion — all ℓ_n with $n > 1$ are determined by ℓ_0 and ℓ_1 and their derivatives. At leading order, the boundary conditions (2.7) and (2.8) yield the equations

$$\varphi_1^s = \ell'_0(\varphi_0^s), \quad (2.17)$$

$$\ell_1(\varphi_0^s) = -\frac{1}{2}(\ell'_0(\varphi_0^s))^2. \quad (2.18)$$

The fact that the asymptotic solutions contain two essentially arbitrary (up to boundary conditions) functions $\ell_0(\varphi)$ and $\ell_1(\varphi)$ might seem peculiar at first glance. However we remind the reader that the initial conditions for a point-like string configuration contain two functions which are also arbitrary up to boundary conditions. Evidently these two initial functions must map onto $\ell_0(\varphi)$ and $\ell_1(\varphi)$ via the equation of motion (2.9). Unfortunately we do not currently see any nice analytic way of relating the initial data for a point-like string to the functions $\ell_0(\varphi)$ and $\ell_1(\varphi)$.

From the above discussion we see that at late times the strings endpoints follow the trajectories

$$x_s(t) = V_s t \quad (2.19)$$

$$u_s(t) = \sqrt{1 - V_s^2} t, \quad (2.20)$$

where $V_s = \cos \varphi_0^*$. These trajectories are simply geodesics in the zero temperature AdS geometry. It is very easy to understand the origin of the asymptotic endpoint geodesic behavior. After a long period of time the presence of the gravity implies that the radial coordinate of the endpoint must increase like $u_s \sim t$. However, by assumption are considering strings whose endpoint motion also scales like $x_s \sim t$ at late times. These two conditions together with the condition that the endpoints move at the speed of light then fixes the asymptotic endpoint motion to be a light-like geodesic.

2. Finite Temperature

Our approach to obtaining finite temperature approximate solutions to the string equations of motion is less systematic than our approach at zero temperature. In particular we do not perform a late time expansion. The reason is simple — at asymptotically late times the string endpoints always fall into the black hole, and consequently the endpoint motion in the spatial directions ceases. This corresponds to the energy loss and thermalization of jets in the dual field theory. The late time behavior of any string solution at finite temperature simply consists of a string of constant spatial extent, whose radial coordinate asymptotically approaches the event horizon.

Instead of performing a $t \rightarrow \infty$ expansion, we construct an asymptotic expansion for a string solution with very high energy. The validity of our expansion will turn out to be equivalent to the statement that the energy density and energy flux on the string are parametrically high. From the field theory point of view this is not surprising. The quark that the string is describing loses energy to the SYM plasma at a rate $dE_{\text{quark}}/dx \sim E^n$ for some $n > 0$. Therefore asymptotically high energy states will deposit a large amount of energy per unit length into the plasma. From the gravitational point of view this corresponds to having a large energy flux and energy density along the string.

Generically the endpoint motion of a falling string is bounded by that of a light-like geodesic which starts at $u = u_0$. It is easy to work out the equations of motion for light-like geodesics in the AdS-BH geometry. They read

$$\left(\frac{dx_{\text{geo}}}{dt}\right)^2 = \frac{f^2}{\xi^2}, \quad (2.21)$$

$$\left(\frac{du_{\text{geo}}}{dt}\right)^2 = \frac{f^2(\xi^2 - f)}{\xi^2} \quad (2.22)$$

where ξ is a constant which specifies the geodesic. Note that for any geodesic which obtains a minimal radial coordinate u_{min} on its trajectory, the parameter ξ must satisfy $\xi^2 > f(u_{\text{min}})$. Dividing Eq. (2.21) by Eq. (2.22)

we see

$$\left(\frac{dx_{\text{geo}}}{du}\right)^2 = \frac{1}{\xi^2 - f}. \quad (2.23)$$

Eq. (2.23) may be integrated to determine the total spatial extent that the geodesic travels. In the limit $\xi^2 \rightarrow f(u_0)$ and $u_0 \rightarrow 0$, this distance scales like u_h^2/u_0 .

We consider string configurations where the spatial component of the string endpoint motion $x_s \approx t$ for times $t \ll u_h^2/u_0$. Under this condition the endpoint velocity in the Minkowski spatial directions will be very close to the local speed of light. Because open string endpoints must always travel at the speed of light, the velocity in the radial direction must therefore be small and correspondingly, the radial coordinate of the string endpoints must change very slowly for times $t \ll u_h^2/u_0$.

Just as at zero temperature, the assumption that the $x_s \approx t$ implies the string must stretch and expand as time evolves. For sufficiently smooth initial conditions² this implies short wavelength perturbations in the initial structure of the string will expand and become long wavelength, resulting in a smooth string profile at late times. Moreover, as the string endpoints separate, the middle of the string must fall rapidly toward the event horizon. In our numerical studies discussed in Section II B, we have found that this typically occurs over a time scale $\Delta t \sim u_h$. This is the time scale for a geodesic with $\xi \ll 1$ to fall into the horizon. We see this for both of the numerically generated string solutions in Figs. 6 and 9. The origin of this behavior can be understood as follows. Consider the string at times shortly after the creation event. It will have expanded to a size $\sim t$. By construction the string will have a very large momentum density in the spatial directions. The momentum density must be very inhomogeneous so that each endpoint can move off in its own direction. As time progresses the parts of the string with the highest momentum density will evolve to be located near the string endpoints. Portions of the string with low momentum density will lag behind the endpoints and fall relatively unimpeded toward the horizon. After the middle of the string falls into the event horizon, the trajectories of the two halves of the string which extend up from the horizon will be uncorrelated. As time progresses, each half of the string will translate along in the spatial directions and the endpoint will slowly fall. We see this nicely for the numerical strings in Figs. 6 and 9.

² Initial conditions where there is an arbitrarily large amount of structure in the string at early times do not have to relax to a smooth string profile after any given amount of time Δt . While the initial structure will be inflated as time progresses, because the string endpoint can only travel a distance $\sim u_h^2/u_0$, one can always cook up initial conditions such that the initial structure never relaxes in this time interval. We do not consider such initial conditions in this paper.

With the above motivation in mind, our starting point for the construction of approximate finite temperature string solutions is to consider a half string which asymptotically approaches the event horizon at spatial distances far from the string endpoint. We look for solutions which approximately translate at constant velocity in the spatial directions. These solutions will be approximately stationary in the rest frame of the string endpoint during the time interval $u_h \ll t \ll u_h^2/u_0$.

We choose worldsheet coordinates $\tau = t$, $\sigma = u$. In these coordinates the embedding functions are determined by one function $x(t, u)$. The domain in the (t, u) plane in which $x(t, u)$ is defined is bounded by a curve $u_s(t)$. This curve corresponds to the trajectory of the string endpoint and is determined by imposing the open string boundary conditions. The equation of motion of $x(t, u)$ is

$$2u(1+fx'^2)\ddot{x} - 2uf(f-\dot{x}^2)x'' - 4ufx'\dot{x}\dot{x}' + 4f(2-f(1-x'^2))x' - 4(3-2f)x'\dot{x}^2 = 0. \quad (2.24)$$

We seek a solution to Eq. (2.24) of the form

$$x(t, u) = x_{\text{steady}}(t, u) + \epsilon x_1(t, u) + \mathcal{O}(\epsilon^2) \quad (2.25)$$

where

$$x_{\text{steady}}(t, u) = \xi t + x_0(u), \quad (2.26)$$

is a steady state solution to the equations of motion with ξ a constant and ϵ is a formal expansion parameter. Similarly, we write

$$u_s(t) = u_0^s(t) + \epsilon u_1^s(t) + \mathcal{O}(\epsilon^2). \quad (2.27)$$

The function $x_1(t, u)$ characterizes the perturbations in the string which have inflated to long wavelengths.

We note that having nontrivial time dependence in $u_s(t)$ does not contradict the steady state assumption in Eq. (2.26). As we shall soon see, the steady state condition implies that $u_0(t)$ must satisfy a geodesic equation.

At leading order in ϵ the equation of motion (2.24) lead to the following equation of motion for $x_0(u)$

$$2uf(\xi^2 - f)x_0'' + 4f^2x_0'^2 + 4[(2-f)f - \xi^2(3-2f)]x_0' = 0. \quad (2.28)$$

The general solution to the above equation is given by functions which satisfy

$$\left(\frac{\partial x_0}{\partial u}\right)^2 = \frac{u^4(\xi^2 - f)}{u_h^4 f^2 (1 - Cf)} \quad (2.29)$$

where C is an arbitrary constant. Before integrating Eq. (2.29), we first determine C by imposing the open string boundary conditions. The reader may note that Eq. (2.29) is the equation of motion for the dragging string of Refs [6, 7]. There, the string obeys a Dirichlet condition at the endpoint and consequently C is found

to be $1/\xi^2$. We will find a different value of C because we solve the problem for different boundary conditions. As a result, we generally obtain a different solution than the string of Refs [6, 7].

With our choice of worldsheet coordinates, the open string boundary conditions are simply

$$G_{MN} \frac{dX^M}{dt} \frac{dX^N}{dt} = 0, \quad (2.30)$$

$$G_{MN} \frac{dX^M}{dt} \frac{\partial X^N}{\partial u} = 0, \quad (2.31)$$

where all quantities are evaluated along the curve $u_s(t)$. At leading order in ϵ these boundary conditions lead to the two equations

$$\left(\frac{\partial x_0}{\partial u}\right)^2 = \frac{\xi^2 - f}{f^2}, \quad (2.32)$$

$$\left(\frac{du_0^s}{dt}\right)^2 = \frac{f^2(\xi^2 - f)}{\xi^2}, \quad (2.33)$$

where all quantities are evaluated along the curve $u_0^s(t)$. Comparing Eq. (2.32) with Eq. (2.29), we see the two equations agree if $C = 1$. Furthermore, comparing Eq. (2.33) with Eq. (2.22), we see that to leading order in ϵ , the string endpoints follow light-like geodesics.

With $C = 1$ Eq. (2.29) may be integrated. Taking the negative root of the equation so that the string profile trails the endpoint, we can find the profile in terms of Appell hypergeometric functions. For the special case of $\xi \rightarrow 1$, $x_0(u)$ reduces to

$$x_0(u) \stackrel{\xi \rightarrow 1}{=} \frac{u_h}{2} \left[\tan^{-1} \frac{u}{u_h} + \frac{1}{2} \log \frac{u_h - u}{u_h + u} \right], \quad (2.34)$$

which is the well know trailing string profile of Refs [6, 7].

Just as at zero temperature, the leading order solution to the string equations of motion is a null string with $\gamma(x_{\text{steady}}) = 0$. Including the $\mathcal{O}(\epsilon)$ correction to the string profile implies $\gamma(x(t, u)) = \mathcal{O}(\epsilon)$. The energy density and energy flux of the string both are proportional to $1/\sqrt{-\gamma}$. Therefore the validity of our asymptotic expansion implies the energy density and energy flux of the string are very high.

It is straightforward to work out the equations of motion for the perturbation $x_1(t, u)$. We do not carry out this exercise here but we simply note that one can show that the perturbations do not become large as time progresses. In particular if ϵ is small, then $\epsilon x_1(t, u)$ remains small for all times. We therefore expect the perturbative expansion in Eq. (2.25) to be valid outside the time window $u_h \ll t \ll u_h^2/u_0$. Indeed as we discuss in Section II B, the agreement between the steady state result and our numerical results agrees for all times $t \sim$ a few u_h .

B. Numerical String Solutions

In addition to studying the asymptotic behaviour of falling strings via the expansions in Section II A, we can

numerically solve the string equations of motion to find the worldsheet for arbitrary initial conditions. These solutions allow us to test the accuracy of the expansions in Section II A and to study string behaviour in the regimes where the expansions do not hold.

For numerical reasons discussed in Ref [6], we have found it convenient to work with the Polyakov action instead of the Nambu-Goto action. The Nambu-Goto action is classically equivalent to the Polyakov action

$$S_P = -\frac{T_0}{2} \int d\tau d\sigma \sqrt{-\eta} \eta^{ab} \partial_a X^M \partial_b X^N G_{MN}, \quad (2.35)$$

where η_{ab} is the worldsheet metric. The equations of motion follow by varying of the action with respect to X^M and η_{ab} . The variation with respect to X^M yields the equation of motion

$$\partial_a [\sqrt{-\eta} \eta^{ab} G_{MN} \partial_b X^N] = \frac{1}{2} \sqrt{-\eta} \eta^{ab} \frac{\partial G_{NP}}{\partial X^M} \partial_a X^N \partial_b X^P, \quad (2.36)$$

together with the open string boundary condition

$$\pi_M^\sigma(\tau, \sigma^*) = 0, \quad (2.37)$$

where

$$\pi_M^\sigma(\tau, \sigma) \equiv \frac{\delta S_P}{\delta \dot{X}^M(\tau, \sigma)} = -T_0 \sqrt{-\eta} \eta^{\sigma a} G_{MN} \partial_a X^N \quad (2.38)$$

and $\sigma = \sigma^*$ at the string endpoints.

The variation of the action with respect to η_{ab} yields the worldsheet constraint

$$\gamma_{ab} = \frac{1}{2} \eta_{ab} \eta^{cd} \gamma_{cd}. \quad (2.39)$$

The constraint equation implies

$$\sqrt{-\gamma} \gamma^{ab} = \sqrt{-\eta} \eta^{ab}, \quad (2.40)$$

which when substituted back into the Polyakov action, easily shows the classical equivalence to the Nambu-Goto action.

One may fix the worldsheet coordinates (τ, σ) by making a choice for the worldsheet metric η_{ab} . Following Ref [6], we choose to fix

$$(\eta_{ab}) = \begin{pmatrix} -\Sigma(x, u) & 0 \\ 0 & \frac{1}{\Sigma(x, u)} \end{pmatrix}, \quad (2.41)$$

where $\Sigma(x, u)$ is a stretching function, which we take to be a function of $x(\tau, \sigma)$ and $u(\tau, \sigma)$ only. With this choice of worldsheet metric, the worldsheet constraints (2.39) read

$$\dot{X} \cdot X' = 0, \quad (2.42)$$

$$\dot{X}^2 + \Sigma^2 X'^2 = 0. \quad (2.43)$$

Since we choose to study point-like initial conditions, we must choose initial data $\dot{X}^M(0, \sigma)$ consistent with the

constraint equation Eq. (2.43) and boundary conditions Eq. (2.37). This is generically satisfied by specifying \dot{t} in terms of \dot{x} and \dot{u} via

$$f \dot{t}^2 = \dot{x}^2 + \frac{\dot{u}^2}{f}, \quad (2.44)$$

in addition to requiring the boundary conditions

$$\dot{t}(\sigma^*) = \dot{x}(\sigma^*) = \dot{u}(\sigma^*) = 0 \quad (2.45)$$

at $\tau = 0$, where σ^* denotes the endpoints of the string.

To choose the functions $\dot{x}(0, \sigma)$ and $\dot{u}(0, \sigma)$ as well as the initial radial coordinate u_0 , we must consider what kind of states we wish to study in the field theory. We first consider the zero temperature theory. As we discuss below in Section III, the endpoints of the strings roughly correspond to the locations of the jets in the boundary field theory. Field theory states with jets that propagate to infinity therefore correspond to falling strings whose endpoints escape to infinity in the spatial directions. We therefore choose to study string initial conditions with enough energy and momentum so that the endpoints separate from each other for all times. In the finite temperature theory, the distance the endpoints can separate is bounded. The field theory states here have a natural quasiparticle description until the jets thermalize. We therefore choose to study initial conditions where we can tune how far the jets travel, i.e. how long the quasiparticle lives before thermalizing.

Beyond these restrictions, the initial conditions are not further constrained by physical requirements. Different initial conditions correspond to different structures of the initial string. What we want to be able to do is to identify aspects of the resulting jets that are universal, but also aspects that depend crucially on the choice of initial conditions.

1. Summary of Results

We have examined a number of initial conditions in the zero and finite temperature cases and in each case have confirmed the approximations in Section II A. In particular, the string endpoints asymptote to geodesics in each geometry and fluctuations along the string at early times are inflated in wavelength as the string falls.

We will now showcase four representative solutions — two at zero temperature and two at finite temperature. The details of how these strings are generated are given below in Section II B 2. The first string we examine is plotted in Fig. 3, with the null string solution $\ell = t$ overlaid. From the figure, we see that the the difference between the null solution and the numeric solution becomes small compared to the size of the string as time progresses. Moreover, we see that the endpoint trajectory is almost completely geodesic.

The above string was generated with rather symmetric initial conditions. To better test the series solution

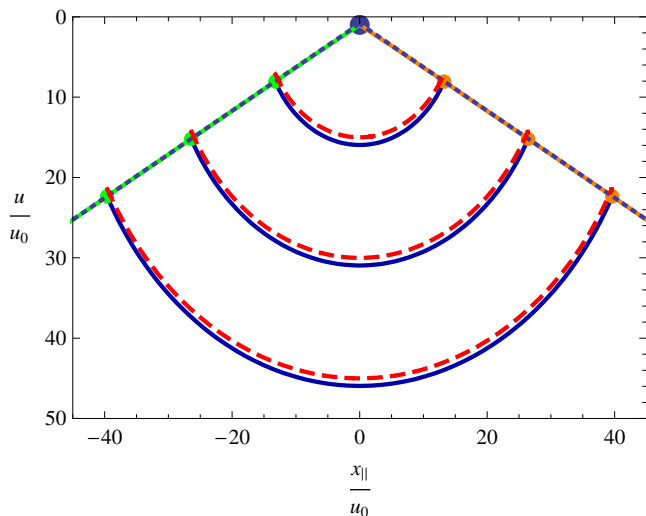


FIG. 3: A falling string at zero temperature. The solid blue curve represents the string at three successive times $t_1 = 15u_0$, $t_2 = 30u_0$, and $t_3 = 45u_0$. The dashed red curve represents the null string approximation $\ell = t$ at the same three times. The orange and green solid curves represent the trajectories of the string endpoints while the dotted blue lines represent the geodesic fit to the endpoint trajectories. The numerical string was generated with the initial conditions in Eq. (2.48) at the large blue dot near the top of the plot. As time progresses, the difference between the null string and the numeric string becomes small compared to the overall size of the string.

Eq. (2.10), we therefore consider a second zero temperature string with large fluctuations at early times. Such a string is shown in Fig. 4. The profile has two large fluctuations at early times that grow in size as the string falls. At these early times, the circular arc solution is not a good fit to the string profile; there is a large perturbation. However as time progresses the short wavelength structure in the perturbation inflates to long wavelengths and the size of the perturbation becomes small compared to the growing size of the string. Again from the figure, one can see that the endpoints approach light-like geodesic trajectories.

According to the expansion given in Eq. (2.10), the difference between any expanding string and the null string $\ell = t$ should have the late time form

$$\ell(t, \varphi) - t = \ell_0(\varphi) + \frac{\ell_1(\varphi)}{t}, \quad (2.46)$$

so for fixed φ , $(\ell(t, \varphi) - t)t$ should be linear in t as $t \rightarrow \infty$. This observation provides a simple test of the form of the asymptotic expansion given in Eq. (2.10). We plot $(\ell(t, \varphi) - t)t$ in Fig. 5 for the above asymmetric string configuration shown in Fig. 4. As is evident from the figure, for fixed φ , $(\ell(t, \varphi) - t)t$ is linear at late times, reinforcing the form of the expansion given in Eq. (2.10).

In the same spirit as with the zero temperature plots above, we exhibit two finite temperature strings — one

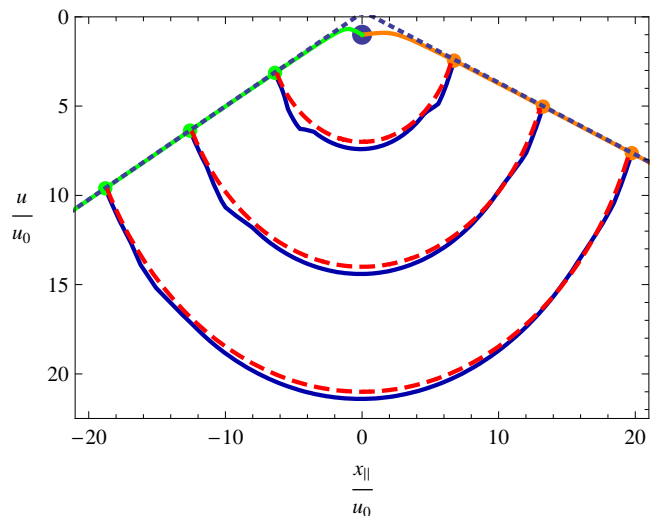


FIG. 4: An asymmetric string at zero temperature generated from the initial conditions Eq. (2.48). The solid blue curve represents the string at three successive times $t_1 = 7u_0$, $t_2 = 14u_0$, and $t_3 = 21u_0$. The dashed red curve represents the null string approximation $\ell = t$ at the same three times. The orange and green solid curves represent the trajectories of the string endpoints while the dotted blue lines represent the geodesic fit to the endpoint trajectories. As time progresses, the perturbations in the string profile inflate and become long wavelength. Correspondingly, the difference between the null string and the numeric string becomes small compared to the overall size of the string.

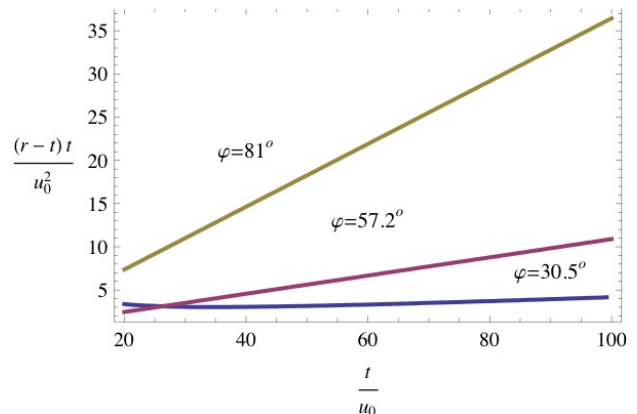


FIG. 5: A plot of the deviation $(\ell(t, \varphi) - t)t$ of the string shown in Fig. 4 from the null string. According to the asymptotic expansion given in Eq. (2.10), for constant values of φ , $(\ell(t, \varphi) - t)t$ should be a linear function of t at late times. The linearity of the plots at late times reinforces the form of the expansion in Eq. (2.10).

smooth string solution and one solution with large fluctuations at early times. A smooth string is shown in Fig. 6. It is a symmetric state about $x = 0$ whose endpoints travel a spatial distance of $19.25/\pi T$. The dotted blue line in the plot represents a geodesic fit to match the stopping distance of the string endpoint. The dashed red

curve shows the corresponding null string plotted on top of the numerical string. As is evident from the figure, the null string fits the numerical solution very well for times $t \sim$ a few u_h .

To see how well the endpoint motion is approximated by a geodesic, we plot $f(dx_s/dt)^{-1}$ in Fig. 7. For a geodesic, this is the constant ξ . The geodesic fit to the stopping distance is plotted in addition to the endpoint data. In the plot, we see that $f(dx_s/dt)^{-1}$ changes by roughly one part in ten thousand over the course of the trajectory of the endpoint. This is completely consistent with the expansion given in Eq. (2.27). In particular, the value of $f(dx_s/dt)^{-1}$ should change by an amount parameterized by ϵ . Evidently, in this case $\epsilon \sim 10^{-4}$.

We also exhibit an asymmetric finite temperature string, as shown at several times in Fig. 9. A close-up of the early-time profile is plotted in Fig. 8. As with the asymmetric zero temperature string in Fig. 4, the early-time fluctuations quickly inflate to long wavelengths. The string quickly relaxes over a time $t \sim u_h$ to match a null string with fluctuations, matching the predictions of Section II A 2.

2. Numerical Details

We generate our numerical strings by solving the string equations of motion with a canned PDE solver: Mathematica's *NDSolve*. We do so with the same technology used in Ref [6]. The crucial difference with the numerical work in Ref [6] is that we must optimize the stretching function on a case-by-case basis. We essentially tune the worldsheet metric to each solution so that gradients along the string are minimized at all times in the string's evolution. We do so with a stretching function of the form

$$\Sigma(x, u) = (x^2 + 1)^m \left(\frac{1 - u}{1 - u_0} \right)^n \left(\frac{u_0}{u} \right)^p. \quad (2.47)$$

Our zero temperature strings can generally be tracked with high accuracy if we only turn on the $\frac{u_0}{u}$ part of this stretching function. Both of the zero temperature strings plotted in this paper simply had $p = 2$ and in each case we were able to track the string down to distances past $10^3 u_0$. The configuration exhibited in Fig. 3 was generated with the initial conditions

$$\dot{x} = 4u_0 \cos \sigma \exp \left[-\frac{1}{2}(1 - \cos^2 \sigma) \right], \quad (2.48a)$$

$$\dot{u} = 2u_0, \quad (2.48b)$$

where we have specified the endpoint locations σ^* to be 0 and π for all of our numerical strings.

Here, we would like to give the reader some intuition about why we chose these initial conditions by highlighting their salient features. First, the exponential factor in \dot{x} allows us to control how much momentum and energy is initially located near the string endpoints. This should roughly correspond to how much momentum and energy

are stored near the quark and antiquark at early times. For this solution, the string therefore has more (but not much more) energy near its endpoints than in the middle. The rest of the initial conditions are chosen to be as simple as possible such that the endpoints fly apart from each other at $t = 0$.

The asymmetric string shown in Fig. 4 was generated with a more complicated set of initial conditions given by

$$\dot{x} = -4u_0 \left(\cos \sigma + \frac{1}{3} \cos 3\sigma \right), \quad (2.49a)$$

$$\dot{u} = u_0 \left(\frac{1}{2} - 2 \cos 4\sigma - \cos 5\sigma \right). \quad (2.49b)$$

Here we chose initial conditions so that the initial velocities along the string, $dx/dt = \dot{x}/t$ and $du/dt = \dot{u}/t$, would have large fluctuations at early times. These evolve to the bumps that inflate in size as the string falls.

Similar to the first zero temperature solution, the initial conditions for the symmetric finite temperature string in Fig. 6 were

$$u_0 = \frac{3}{50} u_h, \quad (2.50a)$$

$$\dot{x} = 626u_0 \cos \sigma \exp \left[-16(1 - \cos^2 \sigma) \right], \quad (2.50b)$$

$$\dot{u} = u_0 \sqrt{f(u_0)} (1 - \cos 2\sigma). \quad (2.50c)$$

In this case, we needed to turn on the other parts of the stretching function Eq. (2.47). For this string, we found the choice $m = 0.6$, $n = 1$, and $p = 2$ to be effective. Also, the initial conditions here are somewhat more extreme than in the zero temperature cases above. Our choice reflects an attempt to make a long-lived string by (i) creating the string near the boundary, (ii) putting most of the energy and momentum near the endpoints, and (iii) giving the endpoints zero initial radial velocity. This last choice allows the string endpoints to travel along an $\xi \approx \sqrt{f(u_0)}$ geodesic for a significant fraction of their trajectory, whereby they travel much further in the spatial direction than an $\xi = 1$ geodesic. See Section IV for more details on this point.

The initial conditions for the asymmetric finite temperature string in Fig. 9 were

$$u_0 = \frac{1}{10} u_h, \quad (2.51a)$$

$$\dot{x} = 30u_0 \left(\cos \sigma + \frac{3}{10} \cos 3\sigma - \frac{1}{25} \right), \quad (2.51b)$$

$$\dot{u} = u_0 \sqrt{f(u_0)} \left(\frac{1}{2} - 2 \cos 4\sigma - \frac{1}{3} \cos 5\sigma \right). \quad (2.51c)$$

We used a slightly different stretching function for this string with $m = 0.7$, $n = 1.5$, and $p = 2$. Here, the initial conditions are similar to those used for the asymmetric zero temperature string of Fig. 4 in that we generate a string that has large fluctuations in the velocities dx/dt and du/dt at small times. We also create the string near the boundary with a large amount of energy near the endpoints so that, like the long-lived finite temperature string in Fig. 9, the endpoints will travel some long distance before falling into the horizon.

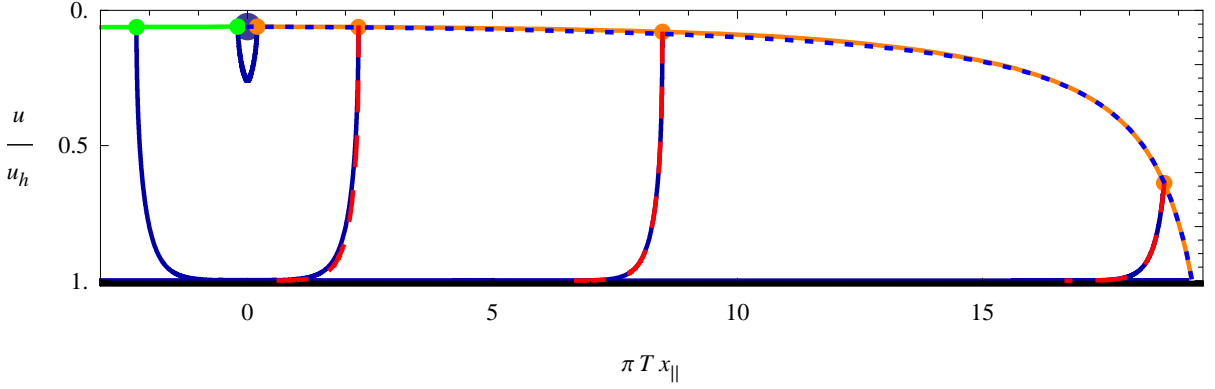


FIG. 6: A symmetric string at finite temperature generated from the initial conditions Eq. (2.50). The string, shown as the solid blue curve, is shown at successive times $t_1 = 1/5\pi T$, $t_2 = 2.3/\pi T$, $t_3 = 8.5/\pi T$, and $t_4 = 18.8/\pi T$ with the corresponding null string, shown as the dashed red curve, plotted at the same times. The solid green and orange curves represent the endpoint trajectories while the dotted blue curve represents the geodesic fit to the endpoint trajectory. The null string agrees very well with the numeric string at times $t \sim$ a few u_h . The geodesic fit to the endpoint trajectory was obtained by matching to the total distance traveled by the endpoint.

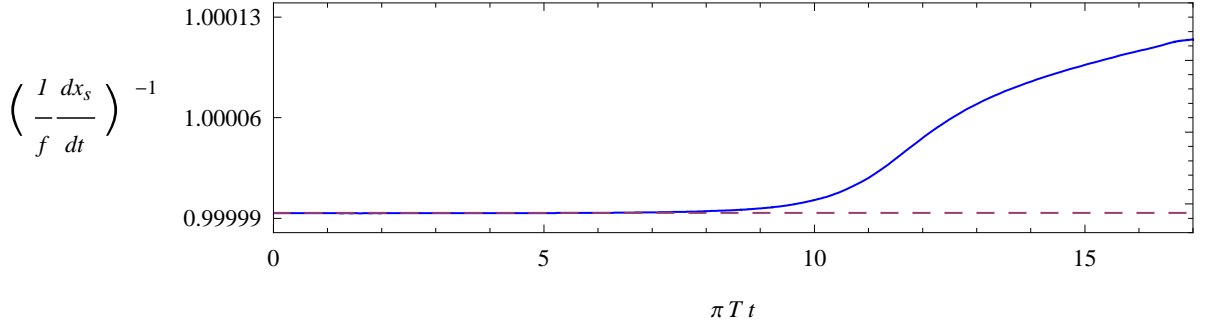


FIG. 7: The quantity $f(dx_s/dt)^{-1}$ for the string of Fig. 6 is plotted with the solid blue line as a function of time. For a geodesic, this is the conserved quantity ξ . We also plot the geodesic fit to the endpoint trajectory with the dashed purple line: $\xi = 0.999994$. As is evident, $f(dx_s/dt)^{-1}$ is approximately constant over the trajectory of the string endpoint. The deviations of $f(dx_s/dt)^{-1}$ from a constant give a measure of the expansion parameter ϵ given in Eq. (2.27).

III. THE ELECTROMAGNETIC PROBLEM AND THE BOUNDARY BARYON DENSITY

In the large N_c limit the action for the $U(1)$ gauge field living on the D7 brane reduces to that of ordinary curved space Maxwell equations. We therefore start with the $N_c \rightarrow \infty$ effective action

$$S = S_{\text{EM}} + S_{\text{int}}. \quad (3.1)$$

The electromagnetic action is given by

$$S_{\text{EM}} = -\frac{1}{4e^2} \int d^5x \sqrt{-G} F_{MN} F^{MN} \quad (3.2)$$

where F_{MN} is the field strength tensor corresponding to the gauge field \mathcal{A}_M and $\frac{1}{e^2} = \frac{N_c}{4\pi^2}$. The interaction action is given by

$$S_{\text{int}} = \int d^5x \sqrt{-G} J \cdot \mathcal{A}. \quad (3.3)$$

where J^M is the current corresponding to the string endpoints.

The equations of motion for the gauge field follow from taking the variation of the action (3.1). The variation of S is

$$\begin{aligned} \delta S = & \int d^5x \sqrt{-G} \delta \mathcal{A}_N \left(\frac{1}{e^2} D_M F^{MN} - J^N \right) \\ & + \frac{1}{e^2} \int_{u=\epsilon} d^4x \sqrt{-G} \delta \mathcal{A}_N F^{5N}. \end{aligned} \quad (3.4)$$

The first term in Eq. (3.4) gives the equations of motion for the gauge field

$$\frac{1}{e^2} D_M F^{MN} = J^N, \quad (3.5)$$

while the surface term gives the boundary baryon current

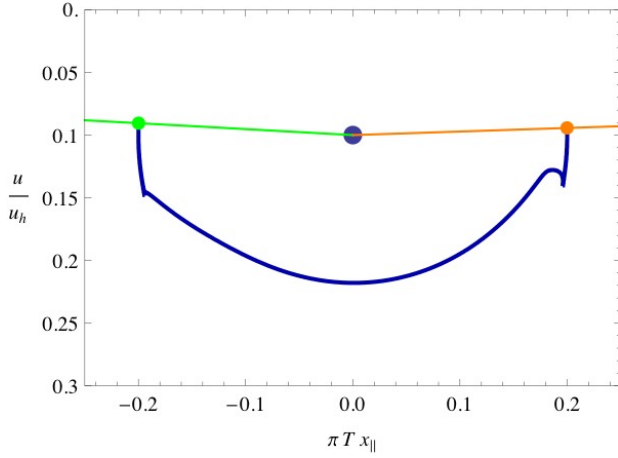


FIG. 8: A closeup of the string in Fig. 9 at time $t = 1/5\pi T$. This plot shows the initial structure in the string which is inflated to long wavelengths at late times.

density

$$j^\mu(t, \mathbf{x}) = \lim_{u \rightarrow 0} \frac{\delta S}{\delta \mathcal{A}_\mu(t, \mathbf{x}, u)}, \quad (3.6)$$

$$= \frac{1}{e^2} \lim_{u \rightarrow 0} \sqrt{-G(t, \mathbf{x}, u)} F^{5\mu}(t, \mathbf{x}, u). \quad (3.7)$$

We note that the above expression for the boundary current density can also be obtained by integrating the equations of motion (3.5) over a gaussian pillbox enclosing the boundary.

From Eq. (3.7) we see that the boundary charge density is determined by the near boundary behavior of the radial component of the electric field

$$E_5 \equiv F_{05}. \quad (3.8)$$

The equations of motion for E_5 can easily be worked out from Eq. (3.5). Introducing a spacetime Fourier transform, we find the following equations of motion for the mode amplitudes $E_5(\omega, \mathbf{q}, u)$

$$E_5'' + A_5 E_5' + B_5 E_5 = S_5 \quad (3.9)$$

where

$$A_5 \equiv \frac{uf' - f}{uf}, \quad (3.10)$$

$$B_5 \equiv \frac{\omega^2 - fq^2}{f^2} - \frac{uf' - f}{u^2 f}, \quad (3.11)$$

$$S_5 \equiv \frac{e^2 L^2 (2J_0 - iu\omega J_5 - uJ_0')}{u^3 f}. \quad (3.12)$$

We may solve Eq. (3.9) with a Greens function $G(u, u')$ constructed out of homogenous solutions

$$G(u, u') = g_>(u_>)g_<(u_<)/W(u') \quad (3.13)$$

where $W(u)$ is the Wronskian of $g_>$ and $g_<$. The appropriate homogenous solutions are dictated by boundary

conditions. The differential operator in (3.9) has singular points at $u = 0$ and $u = u_h$ with exponents 1 and $\pm i\omega u_h/4$. Regularity at the boundary implies $g_<(u) \sim u$ as $u \rightarrow 0$ while the requirement that the black hole not radiate [23] implies that $g_>(u) \sim (u - u_h)^{-i\omega u_h/4}$ near the horizon. The overall normalization of $g_<(u)$ may be fixed by requiring $\lim_{u \rightarrow 0} g_<(u)/u \equiv 1$. From Eq. (3.7) we therefore find that the boundary charge density is given by³

$$\rho(\omega, \mathbf{q}) = \frac{L}{e^2} \int_0^{u_h} du' \mathcal{G}(\omega, \mathbf{q}, u') S_5(\omega, \mathbf{q}, u') \quad (3.14)$$

where

$$\mathcal{G}(\omega, \mathbf{q}, u) \equiv \frac{g_>(\omega, \mathbf{q}, u)}{W(\omega, \mathbf{q}, u)} \quad (3.15)$$

is the Fourier space bulk to boundary propagator.

A. Zero Temperature Baryon Density

At $T = 0$ the AdS radial coordinate ranges over the interval $(0, \infty)$ and $f \equiv 1$. In this case homogenous solutions to Eq. (3.9) may be obtained analytically. The boundary condition on $g_>(u)$ at $u = \infty$ is $\lim_{u \rightarrow \infty} g_>(u) = 0$. We find

$$g_<(u) = uI_0(u\sqrt{q^2 - \omega^2}), \quad (3.16)$$

$$g_>(u) = uK_0(u\sqrt{q^2 - \omega^2}), \quad (3.17)$$

where $I_0(z)$ and $K_0(z)$ are modified Bessel functions. We note that as given in Eq. (3.17), $g_>(u)$ has an ill defined $u \rightarrow \infty$ limit. This can be remedied by giving ω an infinitesimal imaginary part. Causality dictates that the retarded Greens functions be analytic in the upper half ω plane, so the appropriate prescription is to send $\omega \rightarrow \omega + i\epsilon$. With this prescription $g_>(u)$ vanishes at $u = \infty$ for all q and ω . The resulting bulk to boundary propagator is therefore

$$\mathcal{G}(\omega, \mathbf{q}, u) = -K_0(u\sqrt{q^2 - \omega^2}). \quad (3.18)$$

Using the aforementioned $i\epsilon$ prescription, Eq. (3.18) may be Fourier transformed to real space to obtain

$$\mathcal{G}(t, \mathbf{x}, u) = \frac{1}{\pi} \theta(t) \frac{d}{dw} \delta(w), \quad (3.19)$$

where w is defined to be

$$w = -t^2 + \mathbf{x}^2 + u^2. \quad (3.20)$$

The zero temperature real space source for E_5 is

$$S_5 = e^2 L^2 [-\partial_u (J_0/u^2) + \partial_0 J_5/u^2]. \quad (3.21)$$

³ We note that $S_5 \propto \frac{e^2}{L}$ so the baryon density is independent of both e and L as it must be.

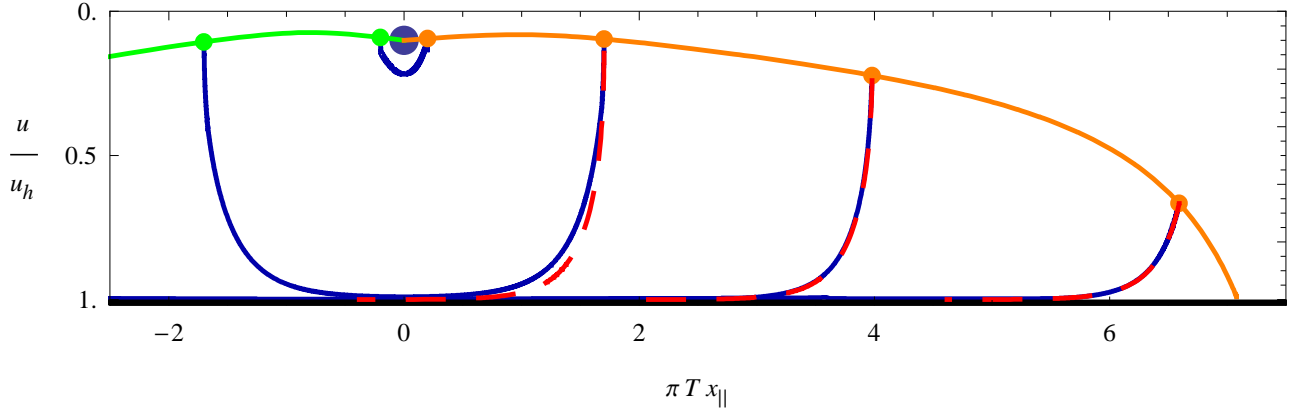


FIG. 9: An asymmetric string at finite temperature generated from the initial conditions Eq. 2.51. The solution and the fitted null string is shown in the same manner as in Fig. 6 at times $t = 1/5\pi T$, $1.7/\pi T$, $4/\pi T$, and $6.7/\pi T$.

Combing the real space version of Eq. (3.14) as well as Eq. (3.19) and (3.21) and integrating by parts, we obtain

$$\rho(t, \mathbf{x}) = L^3 \int du' d^4 x' \left[\partial_{u'} \mathcal{G}(t-t', \mathbf{x}-\mathbf{x}', u') J_0(t', \mathbf{x}', u') + \partial_0 \mathcal{G}(t-t', \mathbf{x}-\mathbf{x}', u') J_5(t', \mathbf{x}', u') \right] \frac{1}{u'^2}. \quad (3.22)$$

Using coordinate time as a parameter for the string endpoint trajectories, the current corresponding to the string endpoints is

$$J^M(t, \mathbf{x}, u) = \theta(t) \sum_s (-1)^s \frac{1}{\sqrt{-G}} \frac{dX_s^M}{dt} \delta^3(\mathbf{x}-\mathbf{x}_s) \delta(u-u_s) \quad (3.23)$$

where the endpoint trajectory is given by $X_s^M(t)$ and the factor of $(-1)^s$ comes from the fact that the string endpoints are oppositely charged. Substituting Eq. (3.23) into Eq. (3.22) and integrating over \mathbf{x}' and u' , we obtain

$$\rho(t, \mathbf{x}) = \sum_s (-1)^s \int dt' \frac{d^2}{dw_s^2} \delta(w_s) \Gamma_s(t, t'). \quad (3.24)$$

where

$$\Gamma_s(t, t') = -\frac{2}{\pi} \theta(t-t') \theta(t') u_s(t') \left[u_s(t') + (t-t') \frac{du_s}{dt'} \right]. \quad (3.25)$$

and w_s is evaluated at

$$w_s = -(t-t')^2 + (\mathbf{x} - \mathbf{x}_s(t'))^2 + (u_s(t'))^2. \quad (3.26)$$

1. Late Time Asymptotics

In general the value of the baryon density at a particular point (t, \mathbf{x}) depends on the history of the sources in the bulk of the AdS geometry. However, the dependence on the history of sources can be reduced if one considers quantities which are averaged in some sense, such as

moments of the baryon density or the angular distribution of baryon number discussed below. Moreover, the fact that the trajectories of the string endpoints asymptotically approach light-like geodesics suggests that the late time behavior of some averaged quantities should be independent of the history of the the bulk sources. We explicitly demonstrate that this is true for the first moment of the baryon density and for the angular distribution of baryon number defined below in Eq. (3.34).

Consider the first moment of the baryon density associated with jet s , the baryonic center of charge position

$$\bar{\mathbf{x}}_s(t) \equiv \frac{\int d^3 x \mathbf{x} \rho_s(t, \mathbf{x})}{\int d^3 x \rho_s(t, \mathbf{x})} \quad (3.27)$$

where $\rho_s(t, \mathbf{x})$ is the baryon density corresponding to a single string endpoint labeled by s . The denominator is simply $\int d^3 x \rho_s(t, \mathbf{x}) = (-1)^{s+1}$. This follows from the fact that the mirror charge induced on the boundary is always opposite of the corresponding source charge in the bulk. From Eq. (3.24) we therefore have

$$\bar{\mathbf{x}}_s(t) = - \int dt' d^3 x \mathbf{x} \frac{d^2}{dw_s^2} \delta(w_s) \Gamma_s(t, t'). \quad (3.28)$$

Shifting integration variables and performing a couple of integrations by parts, we obtain

$$\bar{\mathbf{x}}_s(t) = \pi \int dt' \frac{\partial}{\partial t'} \left[\frac{\mathbf{x}_s(t') \Gamma_s(t, t')}{\dot{Z}_s(t, t')} \right] \frac{\theta(Z_s(t, t'))}{\sqrt{Z_s(t, t')}} \quad (3.29)$$

where we have defined

$$Z_s \equiv (t-t')^2 - (u_s(t'))^2 \quad (3.30)$$

and $\dot{Z}_s \equiv \partial Z_s / \partial t'$.

In the limit $t \rightarrow \infty$ the domain of integration in Eq. (3.29) will be dominated by $t' \sim t$. As discussed in Section IIA 1 the late time behavior of the string endpoint motion asymptotically approaches light-like geodesics. The particular trajectories are given in

Eqs. (2.19)–(2.20). When substituted into Eq. (3.29), these trajectories yield the late time behavior

$$\bar{\mathbf{x}}_s(t) = \mathbf{v}_s t \quad (3.31)$$

where

$$v_s = \frac{1}{V_s} + \left(1 - \frac{1}{V_s^2}\right) \tanh^{-1} V_s, \quad (3.32)$$

and V_s is the asymptotic velocity of the string endpoint in the Minkowski spatial directions. (The directional dependence of \mathbf{v}_s is the same as that of \mathbf{V}_s .) We therefore see that the velocity of the center of baryon density does not generically equal the velocity of the the string endpoint in the spatial directions. However in the $V_s \rightarrow 1$ limit the two velocities do agree. In particular

$$v_s = 1 + \left(1 - \log \frac{2}{1 - V_s}\right) (1 - V_s) + \mathcal{O}((1 - V_s)^2). \quad (3.33)$$

In this limit the string endpoint trajectory approaches a line of constant radial coordinate u and the position of the center of baryon density coincides with the spatial coordinate of the string endpoints.

At zero temperature it is useful to consider the angular distribution of baryon number

$$\frac{dB_s}{d\Omega} \equiv \int_0^\infty r^2 dr \rho_s(t, \mathbf{x}) \quad (3.34)$$

where $r \equiv |\mathbf{x}|$. This quantity is in spirit similar to the jet energy profiles used in collider physics, see e.g. [24, 25]. For localized lumps of baryon density which escape to spatial infinity, this function measures the angular distribution of baryon number of the jet.⁴

From Eq. (3.34) and Eq. (3.24) we have

$$\frac{dB_s}{d\Omega} = (-1)^s \int_0^\infty r^2 dr dt' \frac{d^2}{dw_s^2} \delta(w_s) \Gamma_s(t, t'). \quad (3.35)$$

Using the delta function to carry our the r integral, we obtain⁵

$$\frac{dB_s}{d\Omega} = (-1)^{s+1} \int dt' \frac{\Delta_s(t, t') - 3x_s(t')^2 \cos^2 \theta}{8\Delta_s(t, t')^{\frac{5}{2}}} \Phi_s(t, t') \quad (3.36)$$

where θ is the angle between \mathbf{x}_s and \mathbf{x} and

$$\Delta_s(t, t') \equiv (t - t')^2 - (1 - \cos^2 \theta) x_s(t')^2 - u_s(t')^2 \quad (3.37)$$

⁴ Alternatively, one could measure the angular distribution of baryon number at infinity with the integrated baryon number flux $r^2 \int dt \hat{\mathbf{x}} \cdot \mathbf{j}(t, \mathbf{x})$.

⁵ Technically we should be summing over several zeros of the delta function in Eq. (3.35). However if one assumes $\cos \theta < 0$, then there is only one zero of the delta function with $r > 0$. We consider $\cos \theta < 0$ and obtain the general result for $\frac{dB_s}{d\Omega}$ by analytic continuation.

and

$$\Phi_s(t, t') \equiv \Gamma_s(t, t') \theta((t - t')^2 - x_s(t')^2 - u_s(t')^2). \quad (3.38)$$

In the $t \rightarrow \infty$ limit the integration in Eq. (3.36) will be dominated by times $t' \sim t$. Just as for the center of charge, we may therefore use the asymptotic endpoint trajectories in Eq. (3.36). Substituting the trajectories in Eqs. (2.19)–(2.20) into Eq. (3.36), we find

$$\frac{dB_s}{d\Omega} = (-1)^{s+1} \frac{1 - V_s^2}{4\pi} \int_0^{\frac{\pi}{2}} dt' \frac{tt'(2tt' + 2t'^2 V_s^2 \cos^2 \theta - t^2)}{[t^2 - 2tt' + t'^2 V_s^2 \cos^2 \theta]^{\frac{5}{2}}}. \quad (3.39)$$

Carrying out the integration in Eq. (3.39), we find the remarkably simple result

$$\frac{dB_s}{d\Omega} = (-1)^{s+1} \frac{1 - V_s^2}{4\pi (1 - V_s \cos \theta)^2}. \quad (3.40)$$

From Eq. (3.40) we may compute the average opening angle of the baryon density. A simple calculation shows that for each jet the opening angle is given by

$$\bar{\theta}_s = \frac{\pi}{2V_s} \left(\sqrt{1 - V_s^2} - 1 + V_s \right). \quad (3.41)$$

In the $V_s \rightarrow 1$ limit this becomes

$$\bar{\theta}_s = \frac{\pi \sqrt{1 - V_s}}{\sqrt{2}} + \mathcal{O}(1 - V_s). \quad (3.42)$$

which shows that jets can be made highly collimated and focused. Moreover, from Eq. (3.33), we see the limit where jet are focussed coincides with the limit where the center of baryon density velocity is close to the speed of light.

B. Finite Temperature Baryon Density

At finite temperature we obtain the boundary baryon density by numerically solving the Maxwell equations (3.9). For a given momentum (ω, \mathbf{q}) , the source S_5 defined in Eq. (3.12), is computed by using the electromagnetic currents corresponding to the numerical string solutions discussed in Section II B. In addition, for each (ω, \mathbf{q}) the homogeneous solution $g_>(u)$ is evaluated by numerically integrating the homogeneous differential equation (3.9) (without sources) outward from the horizon. Then the solution $g_<(u)$ is evaluated by numerically integrating the same equations (without sources) inward from the boundary. Given these numerically determined homogeneous solutions, the baryon density is evaluated by numerically performing the radial integrals in Eq. (3.14), with the source S_5 . The subsequent Fourier space baryon density is then numerically Fourier transformed to real space. In what follows, we consider the string generated by the initial conditions given in Eq. (2.50).

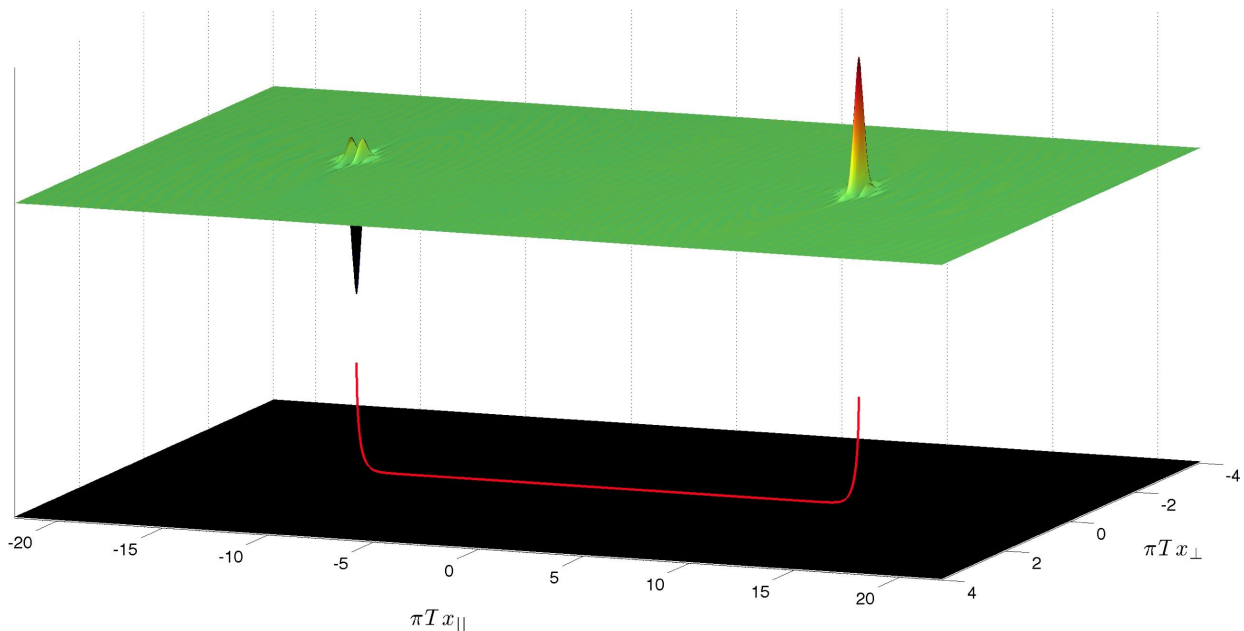


FIG. 10: A snapshot of the string profile and the corresponding baryon density at an instant of time well before thermalization. The black plane represents the event horizon of black hole and the surface on the top represents the boundary baryon density. The red curve is the string and the vertical axis in the plot serves as both the AdS radial coordinate and the magnitude of the baryon density. The baryon density is highly localized above the string endpoints.

Fig. 10 shows a snapshot of a typical finite temperature string/baryon density configuration at a time before thermalization, but much after the initial event where the string was created.⁶ The black plane at the bottom of the figure represents the event horizon of the black hole and the surface on the top of the figure represents the boundary baryon density. The red curve is the string and the vertical axis in the plot serves as both the AdS radial coordinate and the magnitude of the baryon density. As is apparent from the figure, the baryon density is highly localized above the string endpoints. This type of behavior is universal at times t such that $u_h \ll t \ll u_h^2/u_0$ where u_0 is the initial radial coordinate where the string was created.

The fact that the baryon density is localized above the string endpoints is easy to understand from the zero temperature analysis in the previous section. First of all, in the limit where the sources in the bulk are very close to the boundary, the electromagnetic bulk to boundary propagator may be approximated with its zero temperature limit. During the time interval $u_h \ll t \ll u_h^2/u_0$, the radial coordinate of the string endpoint will have not changed much from its initial value of u_0 . In particular, as discussed in Section II A 2, the trajectories of the string endpoints are approximately given by light-like

geodesics in the AdS-BH geometry, so from Eq. (2.23), the rate that the endpoint falls toward the black hole will be suppressed by some power of u_0/u_h .⁷ The source S_5 for the radial component of the electric field E_5 will contain temperature dependence — at leading order in u_0/u_h this temperature dependence is simply the temperature dependence of the trajectories. Therefore, to leading order in u_0/u_h and during the window $u_h \ll t \ll u_h^2/u_0$, we may use the zero temperature expression Eq. (3.31) for the center of the baryon density but with the finite temperature trajectories for the string endpoints. For string configurations whose endpoints propagate very far in the spatial directions, to leading order in u_0/u_h we have $x_s(t) = t$ during the window $u_h \ll t \ll u_h^2/u_0$. From Eq. (3.31) we therefore conclude that $\bar{x}_s(t) = t$ as well, showing that the position of the string endpoints agrees with the center of baryon density.

To elaborate on this behavior, we plot in Fig. 11 the dipole moment of the baryon density and the difference in spatial coordinates of the string endpoints. As is evident from the figure, the two curves agree very well over the vast majority of the string endpoint trajectories. However while the figure demonstrates that as $t \rightarrow \infty$ the dipole moment agrees with the endpoint separation, at

⁶ See <http://www.phys.washington.edu/~karch/Papers/Falling/3D.gif> to download a movie of this event.

⁷ For example, for the special case of $\xi = 1$, Eq. (2.23) implies that $\dot{u}_s(t) \approx \frac{u_0^2}{u_h^2}$ in the window $u_h \ll t \ll u_h^2/u_0$.

times $t \sim u_h^2/u_0$, there is a small discrepancy between dipole moment and the endpoint separation. As we discuss below, the rate that the dipole moment relaxes to a constant is a measure of how the baryon density itself relaxes to its corresponding hydrodynamic modes. This rate will turn out to be much slower than the rate that the endpoints slow down, and this explains the discrepancy in the plot at times $t \sim u_h^2/u_0$.

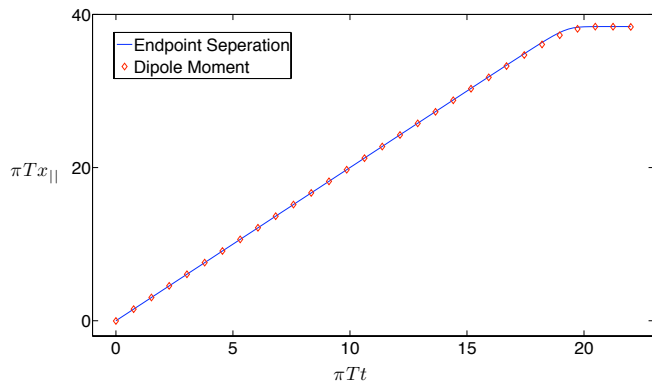


FIG. 11: A plot of the dipole moment of the baryon number and the string endpoint separation in the Minkowski spatial directions. The endpoint separation agrees very well with the dipole moment. There is however a small discrepancy near $t \sim u_h^2/u_0$, which in this plot is $\pi Tt \sim 17$. This is due to the fact that the endpoint velocity slows down at a rate $\sim e^{-4\pi Tt}$ whereas the velocity of the center of baryon density slows down at a rate $\sim e^{-2\pi Tt}$.

Fig. 12 shows a plot of the angular distribution of baryon number

$$\frac{dB_s}{d\theta} \equiv 2\pi \sin\theta \int_0^\infty r^2 dr \rho_s(t, \mathbf{x}). \quad (3.43)$$

for a single jet as a function of both t and opening angle θ . At distances close to the initial creation event $dB_s/d\theta$ is spread out. This just corresponds to the fact the lump of baryon density has a finite width and is very close to the origin.⁸ In particular, it takes a time $t \sim u_0$ for light to reach the boundary after the initial event where the string is created. After a time $t \sim$ a few u_0 , distinct wave packets of baryon density corresponding to each quark will have formed and each packet will have a width $\sim u_0$. From Fig. 12, we see that after a time $t \sim$

⁸ There is a potential numerical effect that might be influencing the spread of the baryon density at early times. When solving the equation of motion (3.9) for the radial component of the electric field $E_5(\omega, \mathbf{q}, u)$, we use a finite Fourier transform range with a cutoff Λ . Correspondingly in position space the numerically generated baryon density cannot have a width that is parametrically smaller than $1/\Lambda$. This effect can potentially make the early time behavior of $dB_s/d\theta$ artificially more spread out than it actually is. We have however checked that the early time behavior of $dB_s/d\theta$ remains as shown in Fig. 12 as Λ is increased.

a few u_h , $dB_s/d\theta$ has settled down to a relatively constant form. As discussed in Section II A 2, the time scale $t \sim u_h$ corresponds to the amount of time it takes for the string to evolve from the point-like initial conditions to the quasi-steady state configuration given in Eq. (2.25). During times in the window $u_h \ll t \ll u_h^2/u_0$, the baryon density slowly spreads out in the transverse directions. In Fig. 12, this manifests itself insofar that the angular width of $dB_s/d\theta$ is approximately constant. Again, in this window of time the temperature dependence in the baryon density will come from that of the trajectories of the string endpoints. That is, to leading order in u_0/u_h the angular width can be computed using the zero temperature expression for the angular distribution of baryon number in Eq. (3.36), but with the temperature dependent endpoint trajectories. The precise result for the opening angle is rather complicated and depends on details of the endpoint trajectory (i.e. the exact value of ξ) so we do not give it here.

At late times, the baryon density spreads out rapidly. In the gravitational theory this corresponds to times in which the string endpoints asymptotically approach the event horizon. As a string endpoint nears the horizon, to an observer on the boundary, the electric fields sourced by the string endpoint will have arbitrarily long wavelengths due to the strong gravitational redshift caused by the black hole. Correspondingly the baryon density induced on the boundary will be diffuse and spread out. From hydrodynamic considerations, one expects that the late time evolution of the baryon density will be that of the diffusion equation

$$(\partial_0 - D\nabla^2) \rho = \Theta \quad (3.44)$$

where $D = 1/2\pi T$ is the baryon density diffusion constant [26, 27] and Θ is a localized source in space and time. Using techniques developed in Refs [28, 29, 30], it is easy to compute the source from the gravitational theory. We have carried out this exercise, and for the symmetric strings discussed in Section II B, found the following simple result

$$\Theta(t, \mathbf{x}) = \mathbf{d} \cdot \nabla \delta^3(\mathbf{x}) \delta(t) \quad (3.45)$$

where \mathbf{d} is the dipole moment of the baryon density which as mentioned above, corresponds to the $t \rightarrow \infty$ limit of the string endpoint separation in the spatial direction. The above result for the source is easy to understand. At leading order in gradients, its form is fixed by the requirement that it be local in space and time and that the dipole moment of the baryon density in the hydrodynamic regime simply be \mathbf{d} .

We now turn to the rate in which dipole moment shown in Fig. 11 relaxes to its final value of \mathbf{d} . The hydrodynamic treatment of the baryon density discussed above always yields a constant dipole moment. Therefore, at late times, any time dependence in the dipole moment is a measure of how quickly the system relaxes to a hydrodynamic description. Generically, one expects that the

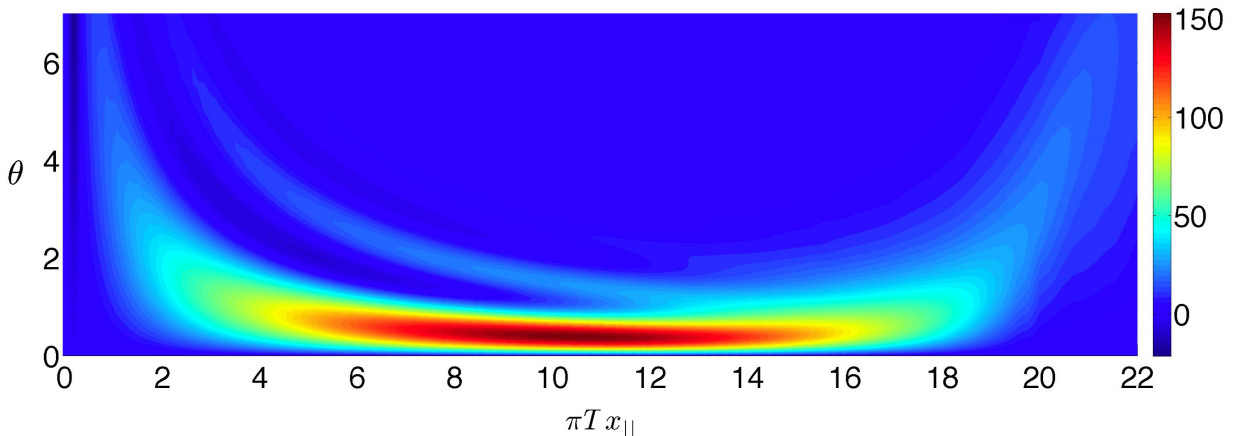


FIG. 12: A plot of $dB_s/d\theta$ for a typical string configuration where the endpoints travel far in the spatial directions. At times $u_h \ll t \ll u_h^2/u_0$, $dB_s/d\theta$ is highly localized about $\theta = 0$. During these times the baryon density wavepacket describes a quasi-particle. Around times $t \sim u_h^2/u_0$, which for this example is $\pi T t \sim 17$, the quasi-particle has lost most of its energy and the resulting jet thermalizes. Correspondingly, the baryon density of the jet spreads out and diffuses at late times. Note that the total baryon number contained in any slice of constant time is unity.

rate that the system relaxes to hydrodynamics will be governed by the imaginary part of the quasinormal modes in the current-current correlator. For $\mathcal{N} = 4$ SYM, these modes were first found in Ref [31] and are given by

$$\omega_n = -2\pi T n(\pm 1 + i), \quad (3.46)$$

where n is a positive integer. We therefore expect the system to relax to hydrodynamics with a characteristic time scale $1/2\pi T$.

As one can easily reason from the geodesic equation (2.21), the rate that the string endpoints slow down as they approach the event horizon is

$$\dot{x}_s(t) = \frac{f}{\xi}, \quad (3.47)$$

so $\dot{x}_s(t) \sim e^{-4\pi T t}$. This rate in fact applies under more general circumstances than for geodesics — any trajectory which is light-like will slow down at this rate near the horizon. Similarly, the rate that the radial coordinate increases is

$$\dot{u}_s(t) \approx f. \quad (3.48)$$

Now suppose the source emits a signal at time t_0 . It will take some time τ for this signal to reach the boundary. After a time Δt the source will have fallen a distance $\Delta s \approx \frac{\dot{u}_s}{f} \Delta t \approx \Delta t$ closer to the horizon. Therefore a signal emitted at time $t_0 + \Delta t$ will take a time $\tau + 2\Delta t$ to reach the boundary. It therefore follows that an observer on the boundary will see the string endpoint velocity in the spatial direction decrease like $e^{-2\pi T t}$. We therefore expect that the velocity of the center of baryon density decrease like $e^{-2\pi T t}$ instead of $e^{-4\pi T t}$. The time scale associated with the decay therefore agrees with the lowest quasinormal mode computed in Ref [31]

The late time behavior of the center of charge can also be computed analytically from the bulk to boundary problem discussed in Section III. We have carried out this analysis and found that the result simply reproduces the geometric optics argument given above.

IV. DISCUSSION

A few remarks about our work are in order. We found that universally the endpoint motion of our strings rapidly settles down to a lightlike geodesic. Not just that, in fact the whole worldsheet approaches a lightlike configuration which we were able to construct analytically. There are two reasons why this was anticipated. For one, the effective string action goes to zero as the string falls. For the zero temperature string, the Nambu-Goto action in AdS is identical to Nambu-Goto in flat space with a position dependent string tension that scales as $\frac{1}{u^2}$. On top of this, the effective string tension also decreases as the string becomes more and more lightlike as it falls. For example, for both for a uniformly translating string $x = vt$ at zero temperature, and the dragging string of [6, 7] at finite temperature, the on-shell action scales as $\sqrt{1-v^2}$. One can again interpret this as a velocity dependent string tension that goes to zero as v goes to 1. Indeed, in our late time configuration each point on the string individually follows a lightlike geodesic. At finite temperature a similar point was also made in [8].

One result we obtained that is perhaps surprising is that in general, the baryon density on the boundary is not localized directly above the string endpoints. In fact from Eq. (3.32) we see that at zero temperature and late times, the spatial velocity V_s of the string endpoints is different than the velocity v_s of the center of baryon density. The two velocities only agree when V_s approaches the speed

of light. In this limit the baryon density on the boundary is localized directly above the string endpoints.

To understand the origin of this behavior it is useful to understand the baryon density induced on the boundary by charges which exactly follow geodesics in the zero temperature AdS geometry. Consider two charges created at $t = 0$, which then move apart on the light-like geodesics

$$x_s(t) = V_s t, \quad (4.1)$$

$$u_s(t) = \sqrt{1 - V_s^2} t + u_0. \quad (4.2)$$

One can readily substitute the above trajectories into Eq. (3.24) and compute the induced boundary baryon density. A remarkable feature of the above geodesics is that the electric fields produced by the charges at times after the creation event do not induce any baryon density on the boundary — all of the baryon density is induced from the initial flash of light produced during the creation event.⁹ Indeed it has been noted in several papers [4, 32] that eternal geodesics, or geodesics which have infinite extent in the past and future, do not induce boundary densities at zero temperature. In the late time limit, the baryon density produced by the initial flash of light is simply

$$\rho_s^{\text{geo}}(t, \mathbf{x}) = (-1)^{s+1} \frac{(1 - V_s^2)}{4\pi r^2 (1 - \hat{x} \cdot \mathbf{V}_s)^2} \delta(t - r). \quad (4.3)$$

This equation describes a focused spherical shell of baryon density expanding at the speed of light. While the shell of baryon density itself expands at the speed of light, the center of baryon density associated with each jet in fact moves at a speed less than the speed of light. This is because the baryon density is expanding in both the transverse and longitudinal directions. This is shown in Fig. 13. As one can easily compute from Eq. (4.3), the velocity of the center of baryon density is given by Eq. (3.32), and is in general not equal to V_s .

At zero temperature, the fact that the baryon density induced by charges moving on geodesics is completely determined by the initial flash of light emitted during the creation event might lead one to suspect that the baryon density induced by string endpoints, whose trajectories only asymptotically approach geodesics, is very sensitive to the initial creation event and not just the asymptotic endpoint trajectories. This intuition is only partially correct. While the value of the baryon density at a particular point (t, \mathbf{x}) might be sensitive to the details of the creation event and the histories of sources in the bulk, certain quantities which are averaged, such as moments of the baryon density, are not sensitive to the detailed history of sources in the bulk. One can explicitly see from Eq. (3.29) that the late time behavior of the center

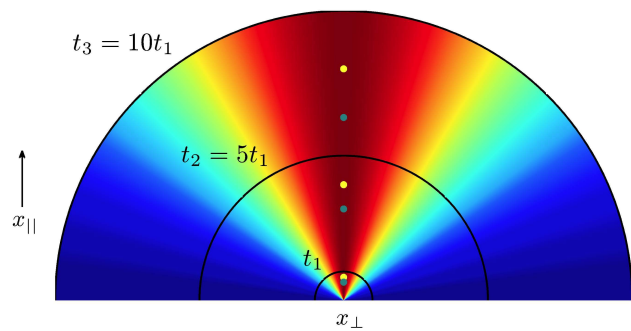


FIG. 13: A plot of the zero temperature baryon density given in Eq. (4.3) at three times t_1 , t_2 , t_3 , with $V_s = 0.8$. At each time, the baryon density is localized on the solid black line. The coloring in the plot shows the angular distribution of baryon number, with red showing a high concentration and blue showing a low concentration. The yellow dots show the spatial position of the charge in the bulk at each time, with the top dot corresponding to time t_3 and the lowest dot corresponding to time t_1 . The blue dots show the position of the center of baryon density at each time with the top dot corresponding to time t_3 and the lowest dot corresponding to time t_1 . As is evident from the plot, the position of the charge in the bulk does not coincide with the center of baryon density. In fact, from Eq. (3.32) they move at different velocities so their separation grows linearly with time.

of baryon density is completely determined by the late time behavior of the endpoint trajectories. Furthermore, one can explicitly see from Eq. (3.36) that the late time angular distribution of baryon number is also completely determined by the asymptotic behavior of the string endpoints. Evidently, the information encoded in the radiation emitted during the times where the string endpoint trajectories are settling down to geodesics contains all of the information about the asymptotic behavior of the endpoint motion.

For the case in which one string endpoint approaches a geodesic with $V_s = 0$, we see from Eq. (3.40) that the corresponding angular distribution of baryon number will be completely isotropic. Of course for a general value of V_s , one can always boost to a frame where this occurs. The angular collimation of baryon density at late times is therefore a consequence of a Lorentz boost.

We note that for the finite temperature string configurations studied in this paper, the center of baryon density did roughly coincide with the location of the string endpoint. We emphasize that the agreement is largely a consequence of the particular states we chose to study. We chose to study string configurations where the string endpoints traveled arbitrarily far in the spatial directions before falling into the black hole. Such configurations naturally have the interpretation of quasi-particles in the boundary field theory. However, to generate such a configuration, the endpoint velocity must reside almost entirely in the spatial directions for most of the trajectory. Furthermore, the endpoints must move at the speed of light. Therefore $V_s \approx 1$ for most of the trajectory.

⁹ More precisely, all of the baryon density comes from differentiating the $\theta(t')$ in Eq. (3.25).

The fact that the baryon density resides over the string endpoint is therefore completely consistent with the zero temperature analysis given above.

It would of course be interesting to study the stress-energy tensor of the jets produced by massless quarks. The stress-energy tensor of very massive quarks moving through a strongly coupled SYM plasma has been studied in Refs [28, 29, 33, 34] while the stress-energy tensor of a meson moving through a strongly coupled SYM plasma has been studied in Ref [35]. However, while we have found that moments of the baryon density and the angular distribution of baryon number are in general insensitive to the exact initial conditions used to create the string, we suspect that the structure of the stress-energy tensor will be very sensitive to the initial conditions. The reason for this is that the strings corresponding to massless quarks in the field theory approach null strings after the initial creation event. As a consequence of this, the determinant of the worldsheet metric, which vanishes for a null string, is strongly dependent on the perturbations which exist on top of the null string. The $5d$ string stress tensor

$$t^{MN}(Y) = -\frac{T_0}{\sqrt{-G}} \int d^2\sigma \sqrt{-\gamma} \gamma^{ab} \partial_a X^M \partial_b X^N \delta^5(Y-X), \quad (4.4)$$

will therefore also depend strongly on the perturbations, and consequently, via the gravitational bulk to boundary problem, the boundary stress tensor will as well. This should be contrasted with the electromagnetic bulk to boundary problem analyzed in this paper, where the electromagnetic currents in the bulk J^M are not sensitive to the perturbations on top of the null strings.

It would be advantageous to find averaged quantities related to the boundary stress-energy tensor, such as moments or jet functions, which are not sensitive to initial conditions. If this is not possible, one can always in principle compute the boundary stress-energy tensor by in some sense averaging over a reasonable set of initial conditions or equivalently, by averaging over perturbations on top of a null string. Whether or not such an averaging procedure is manageable remains to be determined.

At finite temperature one quantity which seems to be somewhat insensitive to the deviations from the null string is the total stopping distance Δx traveled by the quark. At least at the level of the null string approximation, the stopping distance is determined by the initial radial coordinate u_0 and the geodesic parameter ξ . For geodesics which only fall toward the horizon, the stopping distance can be obtained by integrating Eq. (2.23),

$$\Delta x = \int_{u_0}^{u_h} du \frac{1}{\sqrt{\xi^2 - f(u)}}. \quad (4.5)$$

This quantity is however, very sensitive to the value of ξ . For example, consider the case of $\xi = 1$. Then in the $u_0 \rightarrow 0$ limit, Eq. (4.5) integrates to $\Delta x = \frac{u_h^2}{u_0}$. Now consider $\xi = \sqrt{f(u_0)}$ and take $u_0 \rightarrow 0$. This configuration

yields $\Delta x = \frac{\sqrt{\pi}\Gamma(\frac{5}{4})}{\Gamma(\frac{3}{4})} \frac{u_h^2}{u_0} = 1.31 \frac{u_h^2}{u_0}$. Therefore a seemingly small change in ξ can yield a 30% change in Δx . The origin of this behavior is simply that Δx as defined in Eq. (4.5), is not analytic at $\xi = \sqrt{f(u_0)}$. Moreover, $\xi = \sqrt{f(u_0)}$ sets the endpoint velocity in the spatial direction to be the local speed of light, and hence can maximize the total distance traveled.

Based on the above arguments, one might suspect that the deviations from geodesics in the endpoint trajectories might have an important influence of the total distance traveled by the endpoint. From Fig. 7 one can see that the quantity, $f(dx_s/dt)^{-1}$, which is equal to ξ for a geodesic, is in fact not constant. It changes by 1 part in 10^4 over the course of the trajectory of the string endpoint. This is consistent with the perturbative string solutions discussed in Section II A 2. In general, corrections to the endpoint trajectories will be $\mathcal{O}(\epsilon)$. In fact, the actual value that one chooses for ξ is arbitrary up $\mathcal{O}(\epsilon)$ corrections. From Fig. 7 the possible values of ξ range from $\xi - 1 = 6.5 \times 10^{-6}$ to $\xi - 1 \approx -10^{-4}$. For the value of $u_0 = 0.06u_h$ used in the numerical solution shown in Fig. 7, these two values for ξ lead to values for Δx which differ by a factor of two. Therefore, if one wants to approximate the endpoint trajectory with a geodesic, one must carefully choose the value of ξ . However, as shown in Fig. 7, ξ is essentially constant for the first half of the trajectory. It is during this part of the trajectory that the string endpoint is close to the boundary and the formula in Eq. (4.5) is most sensitive to the value of ξ . If one uses the initial value of $\xi - 1 = 6.5 \times 10^{-6}$, then one obtains a distance traveled by the geodesic which differs from the actual distance traveled by the string endpoint by 8%.

Even if one chooses to use the initial value of ξ and approximate the trajectories of the string endpoints with geodesics, relating the parameters ξ and u_0 to the initial quark energy or momentum is in general nontrivial. This was discussed in Ref [8], where the stopping distance of a gluon was considered. The analysis of [8] tried to relate the parameters specifying the geodesic to the initial energy of the string. Without full string solutions only estimates were possible. Ref [8] estimated a stopping distance $\Delta x = c u_h \left(\frac{2E_{\text{string}}}{T\sqrt{\lambda}} \right)^{\frac{1}{3}}$ where $c \approx 1$ and E_{string} is the energy of a string which asymptotically approaches the event horizon. In order to compare this estimate to our numerical strings, we take E_{string} to be half of the initial energy of our point-like strings. This is reasonable as the initial point-like configuration rapidly settles down to a quasi steady state configuration where the center of the string asymptotically approaches the event horizon. For the initial conditions given in Eq. (2.50), this yields $E_{\text{string}} \approx 1167\sqrt{\lambda}T$. Using the estimate of Ref [8], we therefore obtain a stopping distance of $\Delta x \approx 13.3u_h$. The actual distance traveled by the string endpoint is $\Delta x \approx 19.3u_h$. We therefore violate the estimate of Ref [8] by 30%. Consequently, we suspect that the analysis of Ref [8] is incomplete.

Last, we discuss how our results generalize to string configurations which lie in multiple spatial directions. Such string configurations give rise to jets which are in general not back to back. Moreover, such configurations can give rise to additional jets caused by energetic gluons. As discussed in Ref [8], an energetic gluon is represented in gauge/string duality by a kink in a string. It is very easy to extend our analysis to general string configurations. Consider first the case of finite temperature. Suppose we consider a configuration which has in addition to the two jets caused by the string endpoints, N additional gluon jets. Such configurations will have a very inhomogeneous distribution of momentum density in the initial string configuration. Portions of the string with a small momentum density will quickly fall to the horizon over a time scale $t \sim u_h$. After this has happened, the trajectories of each portion of string extending up from the horizon are uncorrelated. The string endpoints and the gluon kinks will then move in arbitrary directions and each portion of the string profile will be very well approximated by steady state string profile. Therefore, the full string profile will look like $2 + N$ trailing strings which are translating in different directions and are connected in a region of characteristic size $\sim u_h$. For times $t \gg u_h$, the baryon density induced by each string endpoint will therefore be virtually identical to that obtained by considering strings which only exist in one spatial direction.

To generalize our zero temperature results, we consider strings whose endpoint position in the spatial directions grows with time like $|\mathbf{x}_s| \sim t$. Such strings will expand as they fall and will also approach a null string configuration. Moreover, the radial coordinate of each endpoint will increase with time like $u_s \sim t$. We can therefore repeat the late-time expansion of Section II A 1 for this general case. Doing so, we find that the light-like boundary condition on each string endpoint forces its trajectory to asymptote to a light-like geodesic. Correspondingly, the angular distribution of baryon number for each jet will again be given by Eq. (3.36). However, there will in general be no correlation between the direction of each string endpoint and the resulting cones of baryon density will thus point in arbitrary directions relative to each other. Moreover, the string asymptotes to a profile given by an arbitrary curve on the 4-sphere $\mathbf{x}^2 + u^2 = t^2$. So as in the finite temperature case, a general falling string at zero temperature may have a number of kinks dual to gluon jets.

V. CONCLUSIONS

We have shown, via the AdS/CFT correspondence, that strings falling in anti de-Sitter space are dual to

jets in large N_c , strongly coupled $\mathcal{N} = 4$ super Yang-Mills theory at zero and finite temperature. Ultimately, we studied the baryon density of these jets. To do this, we obtained the endpoint motion for the dual strings. At zero temperature, a falling string's endpoint always travels a path that asymptotes to a lightlike geodesic. The finite temperature case is more complicated. Here we find that, for strings whose endpoints travel far in the Minkowski spatial directions, the endpoint motion approximates a lightlike geodesic even at early times. We then numerically confirmed both of these results.

Next, we computed properties of the baryon density for these jets. Our results are universal at zero temperature. In particular, two integrals of the baryon density — the center of charge of each jet and the angular distribution of baryon number — are completely determined by the endpoints' asymptotic trajectories. From this, we found that zero temperature jets travel forever and that their baryon density is focused into two cones whose angular dependence is related to the asymptotic motion of the string endpoints via the simple formula Eq. (3.40).

At finite temperature, we see three time scales in the evolution of the baryon density. The first scale is the initial radial coordinate u_0 where the string was created. This scale sets the duration of time it takes light to propagate from the bulk of AdS to the boundary and sets the formation time for the production of quasiparticles. The second scale is the horizon radius u_h . It takes a time $t \sim u_h$ for the string in the bulk to relax to a quasi steady state configuration. The third time scale is u_h^2/u_0 . For times in the window $u_h \ll t \ll u_h^2/u_0$, the string uniformly translates along in the spatial directions and the endpoint slowly falls toward the black hole — the radial coordinate does not change much from its initial value of u_0 . Correspondingly, during these times, the baryon density is highly localized above the string endpoint and is naturally interpreted as the baryon density of a quasi particle. At times $t \sim u_h^2/u_0$, the string endpoint is no longer close to the boundary and the resulting baryon density starts to spread out. This corresponds to the thermalization of the jet. For times $t \gg u_h^2/u_0$ the string endpoint has fallen asymptotically close to the event horizon and the baryon density evolves according to hydrodynamics — it simply diffuses.

Acknowledgments

We thank S.D. Ellis, C.P. Herzog, M.J. Strassler, and L.G. Yaffe, for many useful discussions. This work was supported in part by the U.S. Department of Energy under Grant No. DE-FG02-96ER40956.

[1] S. D. Ellis, J. Huston, K. Hatakeyama, P. Loch, and M. Tonnesmann, *Jets in Hadron-Hadron Collisions*,

Prog. Part. Nucl. Phys. **60** (2008) 484–551,

- arXiv:0712.2447 [hep-ph].
- [2] E. Shuryak, *Why does the quark gluon plasma at RHIC behave as a nearly ideal fluid?*, *Prog. Part. Nucl. Phys.* **53** (2004) 273–303, hep-ph/0312227.
- [3] E. V. Shuryak, *What RHIC experiments and theory tell us about properties of quark-gluon plasma?*, *Nucl. Phys.* **A750** (2005) 64–83, hep-ph/0405066.
- [4] S. Lin and E. Shuryak, *Toward the AdS/CFT Gravity Dual for High Energy Collisions: II. The Stress Tensor on the Boundary*, arXiv:0711.0736 [hep-th].
- [5] M. Chernicoff and A. Guijosa, *Acceleration, Energy Loss and Screening in Strongly- Coupled Gauge Theories*, *JHEP* **06** (2008) 005, 0803.3070.
- [6] C. P. Herzog, A. Karch, P. Kovtun, C. Kozcaz, and L. G. Yaffe, *Energy loss of a heavy quark moving through $N = 4$ supersymmetric Yang-Mills plasma*, *JHEP* **07** (2006) 013, hep-th/0605158.
- [7] S. S. Gubser, *Drag force in AdS/CFT*, *Phys. Rev.* **D74** (2006) 126005, hep-th/0605182.
- [8] S. S. Gubser, D. R. Gulotta, S. S. Pufu, and F. D. Rocha, *Gluon energy loss in the gauge-string duality*, arXiv:0803.1470 [hep-th].
- [9] Y. Hatta, E. Iancu, and A. H. Mueller, *Jet evolution in the $N=4$ SYM plasma at strong coupling*, 0803.2481.
- [10] C. L. Basham, L. S. Brown, S. D. Ellis, and S. T. Love, *Electron - Positron Annihilation Energy Pattern in Quantum Chromodynamics: Asymptotically Free Perturbation Theory*, *Phys. Rev.* **D17** (1978) 2298.
- [11] C. L. Basham, L. S. Brown, S. D. Ellis, and S. T. Love, *Energy Correlations in electron - Positron Annihilation: Testing QCD*, *Phys. Rev. Lett.* **41** (1978) 1585.
- [12] C. L. Basham, L. S. Brown, S. D. Ellis, and S. T. Love, *Energy Correlations in electron-Positron Annihilation in Quantum Chromodynamics: Asymptotically Free Perturbation Theory*, *Phys. Rev.* **D19** (1979) 2018.
- [13] D. M. Hofman and J. Maldacena, *Conformal collider physics: Energy and charge correlations*, arXiv:0803.1467 [hep-th].
- [14] J. Polchinski and M. J. Strassler, *Deep inelastic scattering and gauge/string duality*, *JHEP* **05** (2003) 012, hep-th/0209211.
- [15] M. J. Strassler, *Why Unparticle Models with Mass Gaps are Examples of Hidden Valleys*, arXiv:0801.0629 [hep-ph].
- [16] J. M. Maldacena, *The large N limit of superconformal field theories and supergravity*, *Adv. Theor. Math. Phys.* **2** (1998) 231–252, hep-th/9711200.
- [17] S. S. Gubser, I. R. Klebanov, and A. M. Polyakov, *Gauge theory correlators from non-critical string theory*, *Phys. Lett.* **B428** (1998) 105–114, hep-th/9802109.
- [18] E. Witten, *Anti-de Sitter space and holography*, *Adv. Theor. Math. Phys.* **2** (1998) 253–291, hep-th/9802150.
- [19] J. M. Maldacena, *Wilson loops in large N field theories*, *Phys. Rev. Lett.* **80** (1998) 4859–4862, hep-th/9803002.
- [20] S.-J. Rey and J.-T. Yee, *Macroscopic strings as heavy quarks in large N gauge theory and anti-de Sitter supergravity*, *Eur. Phys. J.* **C22** (2001) 379–394, hep-th/9803001.
- [21] S. S. Gubser, I. R. Klebanov, and A. M. Polyakov, *A semi-classical limit of the gauge/string correspondence*, *Nucl. Phys.* **B636** (2002) 99–114, hep-th/0204051.
- [22] A. Karch and E. Katz, *Adding flavor to AdS/CFT*, *JHEP* **06** (2002) 043, hep-th/0205236.
- [23] D. T. Son and A. O. Starinets, *Minkowski-space correlators in AdS/CFT correspondence: Recipe and applications*, *JHEP* **09** (2002) 042, hep-th/0205051.
- [24] S. D. Ellis, *Collider jets in perturbation theory*, hep-ph/9306280.
- [25] M. H. Seymour, *Jet shapes in hadron collisions: Higher orders, resummation and hadronization*, *Nucl. Phys.* **B513** (1998) 269–300, hep-ph/9707338.
- [26] P. Kovtun, D. T. Son, and A. O. Starinets, *Holography and hydrodynamics: Diffusion on stretched horizons*, *JHEP* **10** (2003) 064, hep-th/0309213.
- [27] R. C. Myers, A. O. Starinets, and R. M. Thomson, *Holographic spectral functions and diffusion constants for fundamental matter*, *JHEP* **11** (2007) 091, 0706.0162.
- [28] P. M. Chesler and L. G. Yaffe, *The wake of a quark moving through a strongly-coupled $N = 4$ supersymmetric Yang-Mills plasma*, arXiv:0706.0368 [hep-th].
- [29] P. M. Chesler and L. G. Yaffe, *The stress-energy tensor of a quark moving through a strongly-coupled $N=4$ supersymmetric Yang-Mills plasma: comparing hydrodynamics and AdS/CFT*, 0712.0050.
- [30] S. S. Gubser and A. Yarom, *Linearized hydrodynamics from probe-sources in the gauge- string duality*, 0803.0081.
- [31] P. K. Kovtun and A. O. Starinets, *Quasinormal modes and holography*, *Phys. Rev.* **D72** (2005) 086009, hep-th/0506184.
- [32] U. H. Danielsson, E. Keski-Vakkuri, and M. Kruczenski, *Vacua, propagators, and holographic probes in AdS/CFT*, *JHEP* **01** (1999) 002, hep-th/9812007.
- [33] S. S. Gubser, S. S. Pufu, and A. Yarom, *Energy disturbances due to a moving quark from gauge-string duality*, *JHEP* **09** (2007) 108, arXiv:0706.0213 [hep-th].
- [34] S. S. Gubser, S. S. Pufu, and A. Yarom, *Sonic booms and diffusion wakes generated by a heavy quark in thermal AdS/CFT*, arXiv: 0706.4307 [hep-th].
- [35] S. S. Gubser, S. S. Pufu, and A. Yarom, *Shock waves from heavy-quark mesons in AdS/CFT*, 0711.1415.